

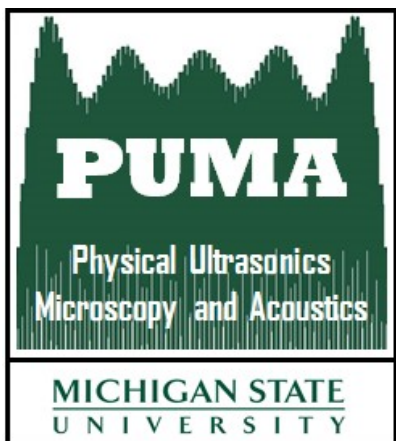
Project report: 2019-2020

Title: Ultrasonic attenuation, backscatter and absorption for microstructure characterization

PI: Dr. Sunil Kishore Chakrapani

Graduate Students: Guillermo Huanes-Alvan, Aakash Khandelwal

Technical contact at EPRI: Thiago Seuaciuc-Osario



Ultrasonic characterization of grade 91 and 92 steel with different heat treatments

G. Huanes-Alvan¹, A. Khandelwal¹, T. Seuaciuc-Osorio³, S. K. Chakrapani^{1,2}

¹*Department of Mechanical Engineering, Michigan State University, East Lansing, Michigan*

²*Department of Electrical and Computer Engineering, Michigan State University, East Lansing, Michigan*

³*Electric Power and Research Institute, Charlotte, North Carolina*

1. INTRODUCTION

A significant portion of failures in grade 91 and 92 steels have been attributed to poor fabrication that results from a high production variability. Developing a nondestructive technique that is capable of distinguishing between steels with microstructural characteristics corresponding to acceptable and non-acceptable mechanical performance. Such a technique could potentially be used in a quality control scenario as well as to assess the condition of installed components.

Ultrasonic wave propagation characteristics such as attenuation, backscatter and absorption are influenced by the microstructure characteristics of the specimen, such as grain size and porosity, in a frequency-dependent manner. Therefore, the frequency-dependent parameters describing these phenomena may provide a volumetric way to assess the specimen's microstructure.

The scope of this work is comprised of obtaining frequency-dependent ultrasonic attenuation, backscatter and absorption measurements on the EPRI sample inventory; processing the data to extract features or metrics that can potentially be used to estimate the specimen's microstructure; and reporting the results.

The main objective of this work is to investigate whether potential features or metrics extracted from frequency-dependent ultrasonic attenuation, backscatter and absorption measurements can be correlated with the specimen's microstructure characteristics in order to classify the specimen as acceptable or not.

2. MATERIALS AND EXPERIMENTAL DETAILS

2.1.1. Materials: Tube samples

To assess the ability of the method, 8 different heat treatments were chosen. A total of 16 samples were used for the study, with 8 known samples, and 8 blind samples. The objective is to correlate the response between the known and unknown samples to predict the heat treatment of the blind samples. Table 1 shows the dimensions of the tube samples.

Table 1. Tubes dimensions

| | Quantity | OD (in) | Wall Thickness (in) | Axial Length (in) | Angular Section |
|----------------------|-----------------|----------------|----------------------------|--------------------------|------------------------|
| Tubes | 16 | 2 | 0.165 | 12 | 360° |
| Pipe Sections | 8 | 18 | 1.5 | 9 | ~60° |

The different heat treatment conditions with their hardness values are shown in Table 2. The blind set of samples are named B1 to B8, and the known heat treatments are name accordingly.

Table 2. Tubes heat treatment conditions.

| Condition | Heat Treatment | Target Hardness (HV 5.0) | Actual Median Hardness |
|------------------|-----------------------|---------------------------------|-------------------------------|
| As received | None | 215 | 220 |

| | | | |
|---------------------|----------------------------------|-----|-----|
| Normalized | 1050°C/0.5h/AC | 425 | 428 |
| Normalized Tempered | + 1050°C/0.5h/AC + 775°C/2h/AC | 215 | 208 |
| Tempered | 790°C/2h/AC | 195 | 207 |
| Over-Tempered | 790°C/10h/AC | 185 | 198 |
| Fully Ferritic | 950°C/0.5h + cool to 760°C/3h/AC | 160 | 147 |
| HAZ | 900°C/1m/AC | 300 | 405 |
| HAZ + Tempered | 900°C/1m/AC + 775°C/2h/AC | 215 | 170 |

2.2.1. Ultrasonic characterization: attenuation parameter

The ultrasonic attenuation coefficient is a frequency dependent parameter that quantifies the losses of acoustic energy of an ultrasonic wave traveling through a sample of a specific material. The attenuation of the samples was measured using planar transducers, 30MHz-0.25in diameter for the tubes and 20MHz-0.25in for the pipe-sections. The 30MHz transducer is a high-frequency transducer that has a permanent fused silica delay line of 4.45 μ s.

The experiments with the tubes were done with a setup shown in Figure 1, similarly Figure 2 shows the setup for the pipe-sections. As the tubes and pipe-sections have a curved surface, diffraction corrections specific to the curvature have to be developed. This work focuses solely on differentiating the tubes and pipe-sections, and since all the samples are geometrically similar, the diffraction correction was not chosen. The expression in Eq. 3 was chosen to obtain the attenuation coefficient as a function of frequency.

$$\alpha_s = \frac{1}{2x_s} \ln \left(\left| \frac{BW 1(f)}{BW 2(f)} \right| * R_{sw}^2 \right) \dots \text{(Eq. 3)}$$

Where, $BW 1$ and $BW 2$ are the amplitudes of the 1st and 2nd back-wall echoes, respectively, x_s is the thickness of the tube wall, R_{sw} , is the reflection coefficients at the interface of specimen-water.

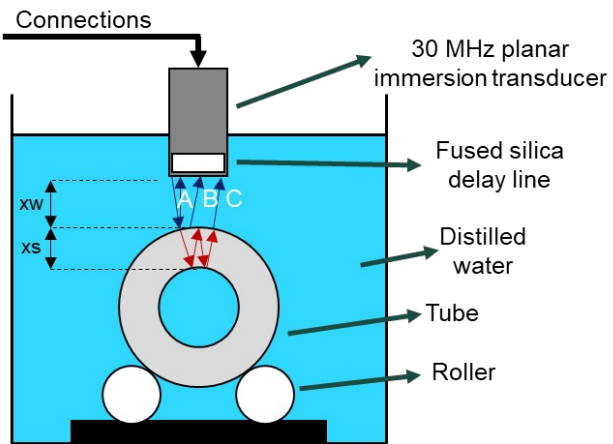


Fig 1: Schematic of the immersion setup for the tubes

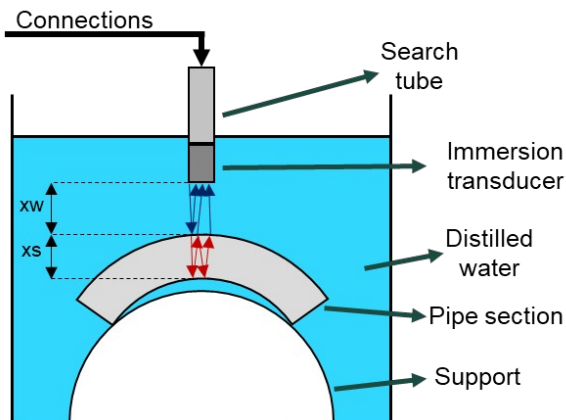


Fig 2: Schematic of the immersion setup for the pipe-sections

2.2.2. Backscatter coefficient

For ultrasonic backscatter coefficient, a focused 30MHz transducer, 0.25inch diameter and 1.25in focal length was focused at mid-plane of the cross section of the tube to get maximum backscatter between the top surface and the mid-plane. The backscatter of the pipe-sections was measured using the same transducer used for the attenuation measurement, 20MHz-0.25in. The backscatter region was determined from the region between the front-wall and the first back-wall (see Fig. 2). The routine followed to obtain the backscatter RMS term is shown in Fig. 2.

Similarly, as with the attenuation coefficient, the curvature of the tubes required a correction to obtain the final backscatter coefficient. Since this is a comparative study, this step was ignored. Instead, the expression in Eq. 7 was applied to obtain the backscatter noise in frequency domain.

$$|\Gamma_{sample}(f)| = \sqrt{\frac{\sum_{i=1}^n |\Gamma_i(f)|^2}{n}} \dots (\text{Eq. 7})$$

Where $|\Gamma_i(f)|$ is the FFT of the windowed backscatter region in time-domain for the datapoint “*i*” of the sample and “*n*” is the number of datapoints (or scan positions) of the sample.

The RMS in the transducer frequency bandwidth was applied to obtain the backscatter term per scan position. The windowed part of the A-Scan was transformed into frequency domain, followed by windowing the frequency domain response between 10MHz – 40MHz. The final backscatter term only has the root mean square (RMS) over the frequency domain, this value was calculated for each datapoint:

$$\Gamma_{iRMS} = \sqrt{\frac{\sum_{f=10\text{MHz}}^{f=40\text{MHz}} |\Gamma_i(f)|^2}{m}} \dots (\text{Eq. 8})$$

Where “*m*” is the number of frequency discrete points from 10 to 40 MHz.

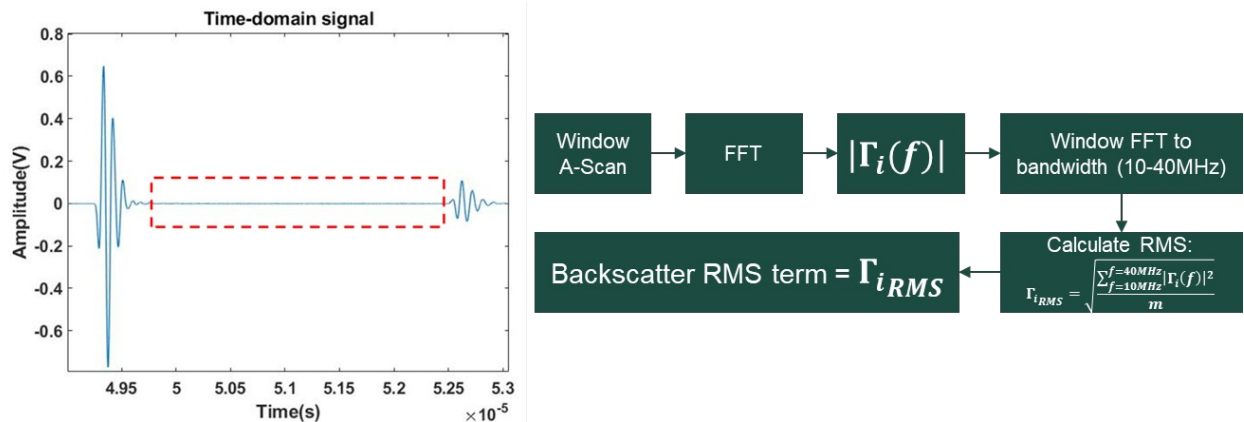


Fig 3. Backscatter region in time domain between front-wall and back-wall echoes.

2.2.3. Absorption measurement

The primary difference between the diffuse field measurement and other techniques is the long acquisition time in the diffuse field measurements. The current set of measurements used two 1 MHz contact transducers held a constant distance of 71 mm apart by means of a fixture and pressed onto the surface of the sample by means of a stand. Fig. 3 shows a schematic of the setup for the tube samples. The same fixture and setup was used for the pipe cross-sections and whole pipe sections. Care was taken to place the transducers in a way that the line joining the contact points was along the axis of the tube or the presumed axis of the pipe. For the pipe cross-sections, the transducers were placed arbitrarily on the flat surface. The excitation was provided to one of the transducers by means of a square wave pulser, and the output waveform recorded at the second transducer. The measurement was performed at 12 angular locations (30° apart) for each tube sample. 10^6 data values were recorded for each location over a total time of 5 ms. For the pipe cross-sections, which were much smaller, 3 readings were recorded for each sample for an acquisition time of 2 ms. For the whole pipe sections, 5-9 readings were recorded per sample, again for a total acquisition time of 5 ms. The data processing routine is shown in Appendix 5. The method follows the earlier work by Panneta.

3. RESULTS:

Since each scan datapoint contained echoes of the front-wall, 1st and 2nd backwall, the velocities of each tube and pipe-section sample were calculated using the peak time-of-flight of the backwalls. These results are shown in Table 3 and Table 4 for the tubes and pipe-sections, respectively.

Table 3. Tubes longitudinal velocities

| TUBE SAMPLE | LONGITUDINAL VELOCITY (m/s) |
|---------------------|-----------------------------|
| AS RECEIVED | 5880.60 ± 75.20 |
| NORMALIZED | 5794.49 ± 85.64 |
| NORMALIZED+TEMPERED | 5815.08 ± 62.77 |
| TEMPERED | 5902.96 ± 39.68 |
| OVER TEMPERED | 5879.93 ± 30.59 |
| FERRITIC | 5845.88 ± 64.01 |
| HAZ | 5869.40 ± 60.69 |
| HAZ+TEMPERED | 5834.46 ± 78.66 |
| B1 | 5801.91 ± 88.27 |
| B2 | 5852.25 ± 92.87 |
| B3 | 5790.53 ± 77.53 |
| B4 | 5764.01 ± 54.81 |
| B5 | 5830.32 ± 87.92 |
| B6 | 5878.79 ± 48.83 |
| B7 | 5795.70 ± 87.08 |
| B8 | 5785.40 ± 86.35 |

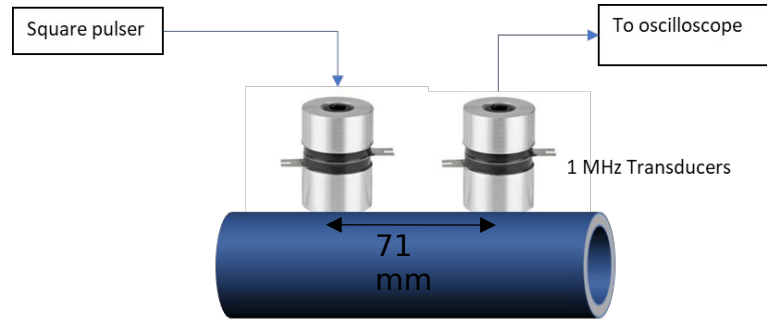


Fig 4: Schematic of the setup for absorption measurement; a similar setup was used for the pipe sections.

Table 4. Pipe-sections longitudinal velocities

| TUBE SAMPLE | LONGITUDINAL VELOCITY (m/s) |
|---------------------|-----------------------------|
| AS RECEIVED | 6269.03 ± 33.99 |
| NORMALIZED | 6180.29 ± 23.20 |
| NORMALIZED+TEMPERED | 6362.94 ± 36.80 |
| TEMPERED | 6295.34 ± 21.44 |
| OVER TEMPERED | 6319.43 ± 28.05 |
| FERRITIC | 6255.22 ± 60.74 |
| HAZ | 6197.58 ± 25.70 |
| HAZ+TEMPERED | 6204.51 ± 40.13 |

3.1. Ultrasonic attenuation:

The attenuation parameter was measured using line scans along the length of the sample. This dataset would typically result in a C-scan image. These results are presented in Appendix 3. However, for a quantitative comparison, a single parameter is necessary. Therefore, the attenuation coefficient was average over approx. 3000-4000 points on each sample. The average attenuation coefficient calculated using this process is shown in Fig. 5 and 6 for the tubes and in Fig. 7 for the pipe-sections. The curves for the known set of samples are shown in Fig. 5 and the blind batch is shown in Fig. 6. The frequency range chosen for presentation is based on the smallest comparable bandwidth of the entire set of results. While these results show a difference, it is important to quantitatively distinguish between them. So, a curve fitting algorithm was used to fit the alpha curves and the fitting parameters were used to compare the results, which will be presented in the discussion section.

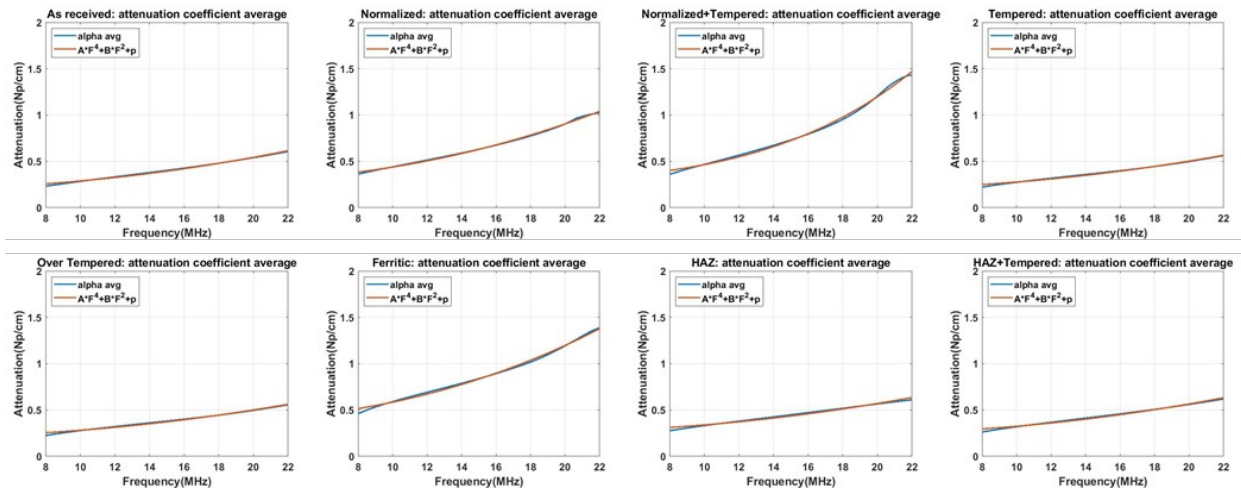


Fig. 5: Attenuation coefficient vs frequency for the known TUBE samples.

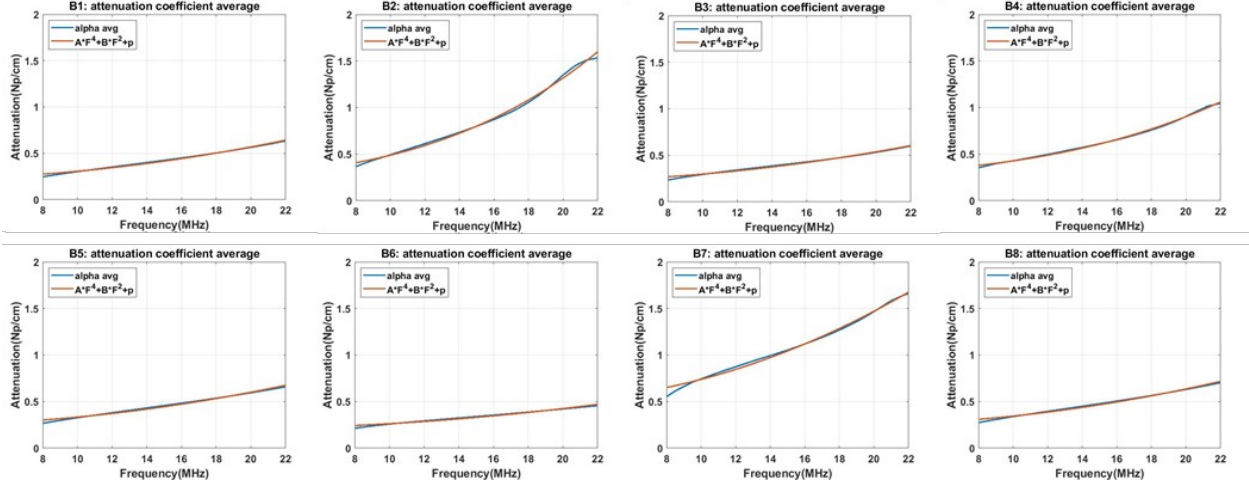


Fig. 6: Attenuation coefficient vs frequency for the blind TUBE samples.

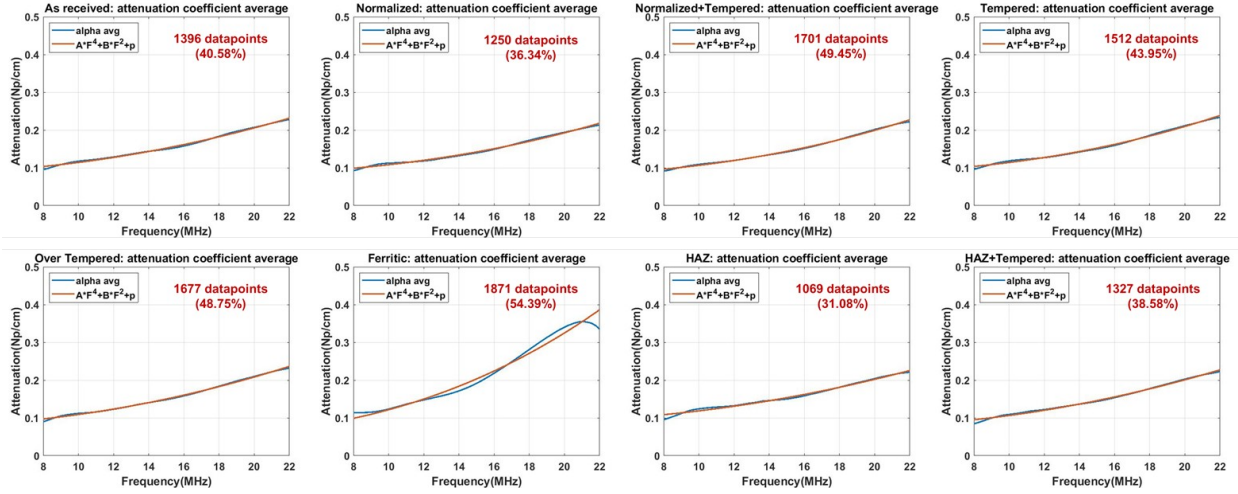


Fig. 7: Attenuation coefficient vs frequency for the PIPE-SECTION samples.

3.2. Ultrasonic backscatter:

The ultrasonic backscatter results for all 16 tube samples are listed in Table 5 and shown in the plot in Fig. 8. Similarly, Table 6 and Fig. 9 shows the results for the pipe-sections. The backscatter term gives us a

| | Backscatter rms | | | Backscatter rms | |
|--------------------|-----------------|--------|-----------|-----------------|--------|
| | avg | std | | avg | std |
| As received | 0.0179 | 0.0038 | B1 | 0.0175 | 0.0042 |
| Normalized | 0.0253 | 0.0054 | B2 | 0.0240 | 0.0057 |
| Norm+Temp | 0.0270 | 0.0082 | B3 | 0.0134 | 0.0028 |
| Tempered | 0.0190 | 0.0042 | B4 | 0.0146 | 0.0031 |
| Over Temp | 0.0253 | 0.0057 | B5 | 0.0182 | 0.0040 |
| Ferritic | 0.0201 | 0.0051 | B6 | 0.0148 | 0.0031 |
| HAZ | 0.0156 | 0.0034 | B7 | 0.0300 | 0.0087 |
| HAZ+Temp | 0.0227 | 0.0063 | B8 | 0.0269 | 0.0062 |

Table 5: Backscatter term for various TUBE samples

quantitative measure of the ultrasonic scattering. These results will further be used to quantitatively compare between the samples.

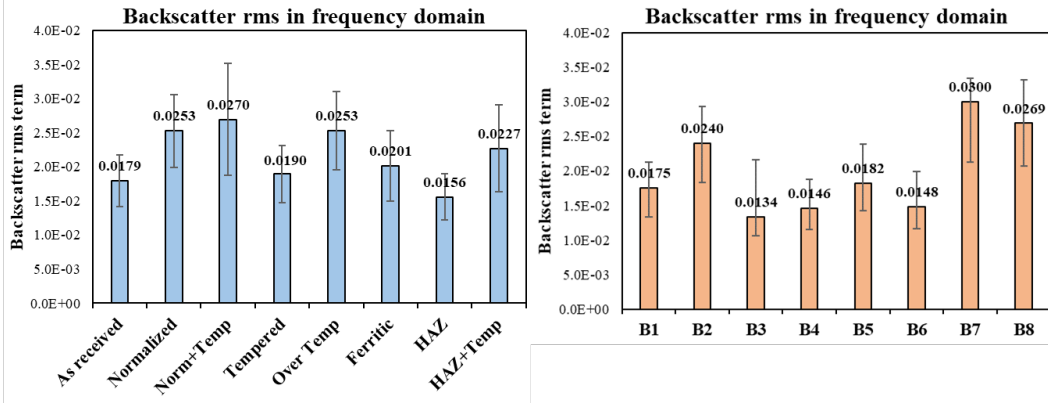


Fig. 8: Backscatter term for various TUBE samples.

| Backscatter rms | |
|--------------------|--------|
| As received | 0.0272 |
| Normalized | 0.0195 |
| Norm+Temp | 0.0230 |
| Tempered | 0.0279 |
| Over Temp | 0.0197 |
| Ferritic | 0.0359 |
| HAZ | 0.0230 |
| HAZ+Temp | 0.0225 |

Table 6: Backscatter term for the PIPE-SECTIONS

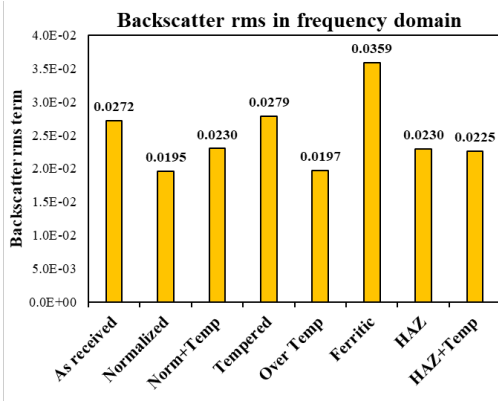


Fig. 9: Backscatter term for the PIPE-SECTIONS.

3.3. Absorption measurements:

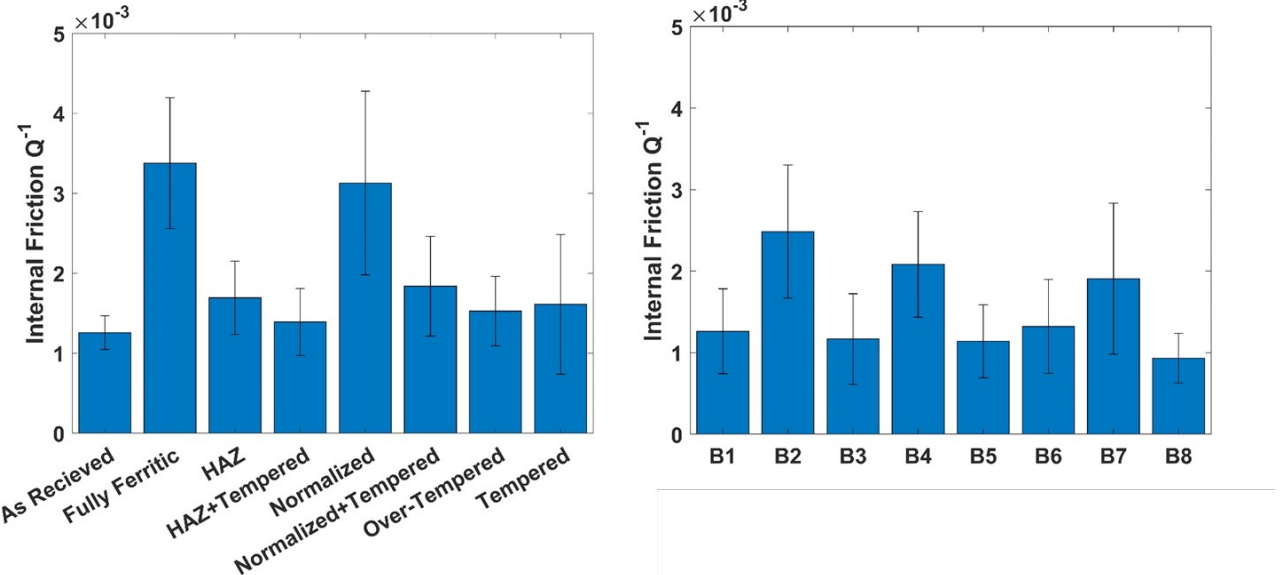


Fig. 10: Absorption measurement (Q^{-1}) for different tube samples.

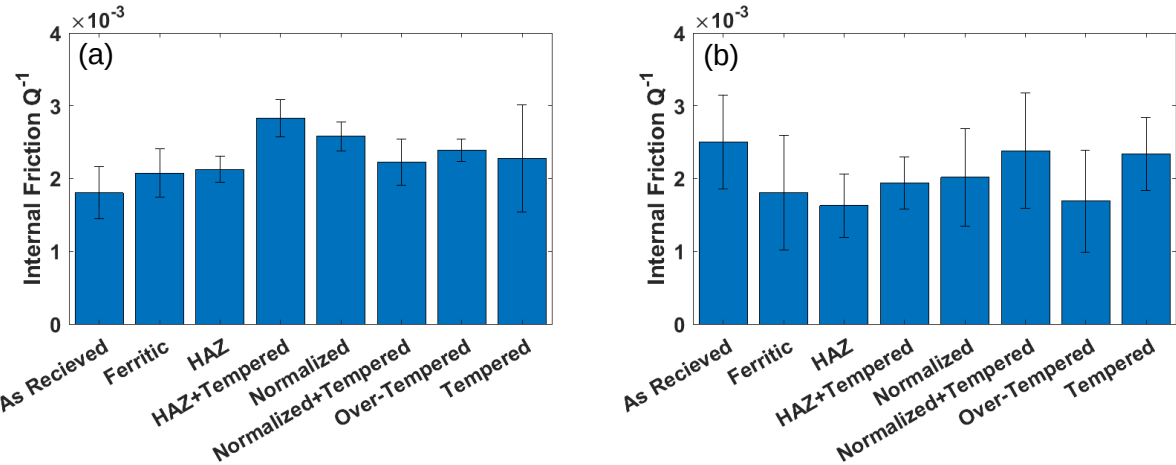


Fig. 11: Absorption measurement (Q^{-1}) for different (a) Pipe Cross-sections, and (b) Whole Pipe Sections.

The internal friction (Q^{-1}) measured using the setup described earlier, and shown in Fig. 7. The time window length chosen for the analysis was 50 μ s, with a frequency window length of 50 kHz and frequency range of 1-3 MHz within which the internal friction was constant with frequency. Interestingly, the results in Fig. 7 shows that at least 2 to 3 tube samples standout compared to rest of the tube samples within both the blind and the known sets. However, for the pipe cross-sections and pipe sections, the difference in the computed Q^{-1} value between samples was not as pronounced. The order of magnitude of the Q^{-1} was the same across all sets of samples.

4. DISCUSSIONS

4.1. Attenuation

The average attenuation coefficient per sample was fitted with the model ($\alpha = Af^4 + Bf^2 + p$) in the 8 to 22 MHz range. The parameter A will be related to scattering, B will be related to absorption, and the

parameter p will account for residual effects which are not corrected for, for example diffraction effects in the curved specimens.

Table 7: Curve fitting results for attenuation coefficient for the TUBES

| | A | B | p |
|--------------------|----------|----------|----------|
| As received | 4.43E-13 | 8.51E-04 | 2.03E-01 |
| Normalized | 1.44E-07 | 1.48E-03 | 2.88E-01 |
| Norm+Temp | 2.07E-06 | 1.41E-03 | 3.02E-01 |
| Tempered | 2.59E-13 | 7.51E-04 | 2.02E-01 |
| Over Temp | 3.99E-13 | 7.31E-04 | 2.08E-01 |
| Ferritic | 2.67E-07 | 1.91E-03 | 3.91E-01 |
| HAZ | 4.20E-14 | 7.72E-04 | 2.62E-01 |
| HAZ+Temp | 4.23E-13 | 8.02E-04 | 2.44E-01 |
| B1 | 4.41E-13 | 8.75E-04 | 2.19E-01 |
| B2 | 1.52E-06 | 2.01E-03 | 2.73E-01 |
| B3 | 4.27E-13 | 7.99E-04 | 2.18E-01 |
| B4 | 7.58E-07 | 1.21E-03 | 2.99E-01 |
| B5 | 3.97E-13 | 8.90E-04 | 2.45E-01 |
| B6 | 1.35E-12 | 5.41E-04 | 2.09E-01 |
| B7 | 4.82E-13 | 2.44E-03 | 4.95E-01 |
| B8 | 4.42E-12 | 9.72E-04 | 2.47E-01 |

The results of curve fitting processing for the tubes and pipe-sections are listed in Table 7 and Table 8, respectively. The alpha curves of all the samples are plotted together in Fig. 12 for the tubes and in Fig. 13 for the pipe-sections, and each term from the curve fitting process has been plotted for the known and blind set of samples in Fig. 12.

As can be seen from the figure, only 3 samples in the known batch have a quartic term, i.e. A. The quadratic contribution in general is much higher for most of the samples. To show this better. From Fig. 14 & 15, it can be seen that few samples standout compared to the others.

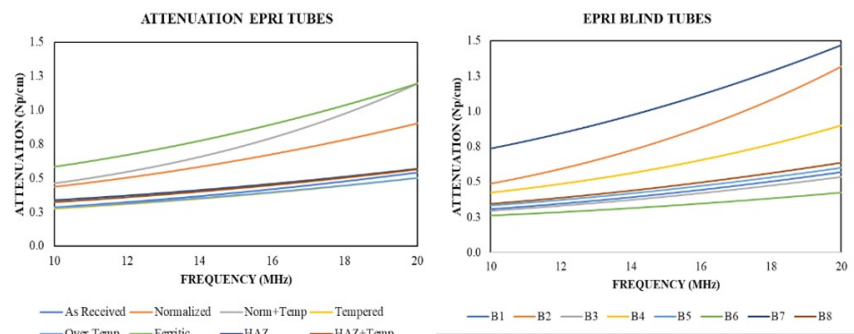


Fig 12: Attenuation coefficient for known and blind TUBES.

Table 8: Curve fitting results for attenuation coefficient for the PIPE-SECTIONS

| | A | B | p |
|--------------------|----------|----------|----------|
| As received | 1.11E-08 | 2.99E-04 | 8.43E-02 |
| Normalized | 6.43E-08 | 2.49E-04 | 8.27E-02 |
| Norm+Temp | 6.88E-08 | 2.74E-04 | 7.85E-02 |
| Tempered | 7.71E-08 | 2.79E-04 | 8.55E-02 |
| Over Temp | 1.44E-08 | 3.24E-04 | 7.65E-02 |
| Ferritic | 1.40E-07 | 6.07E-04 | 5.95E-02 |
| HAZ | 2.26E-10 | 2.78E-04 | 9.09E-02 |

| | | | |
|-----------------|----------|----------|----------|
| HAZ+Temp | 2.01E-13 | 3.15E-04 | 7.49E-02 |
|-----------------|----------|----------|----------|

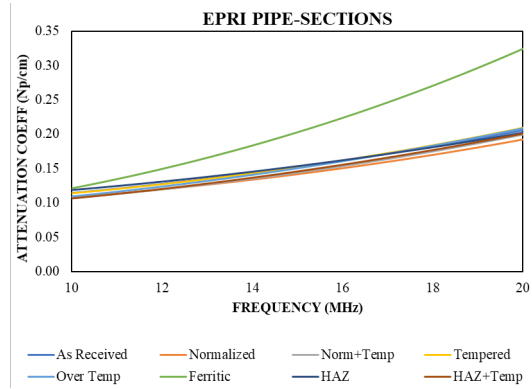


Fig 13: Attenuation coefficient for pipe-sections.

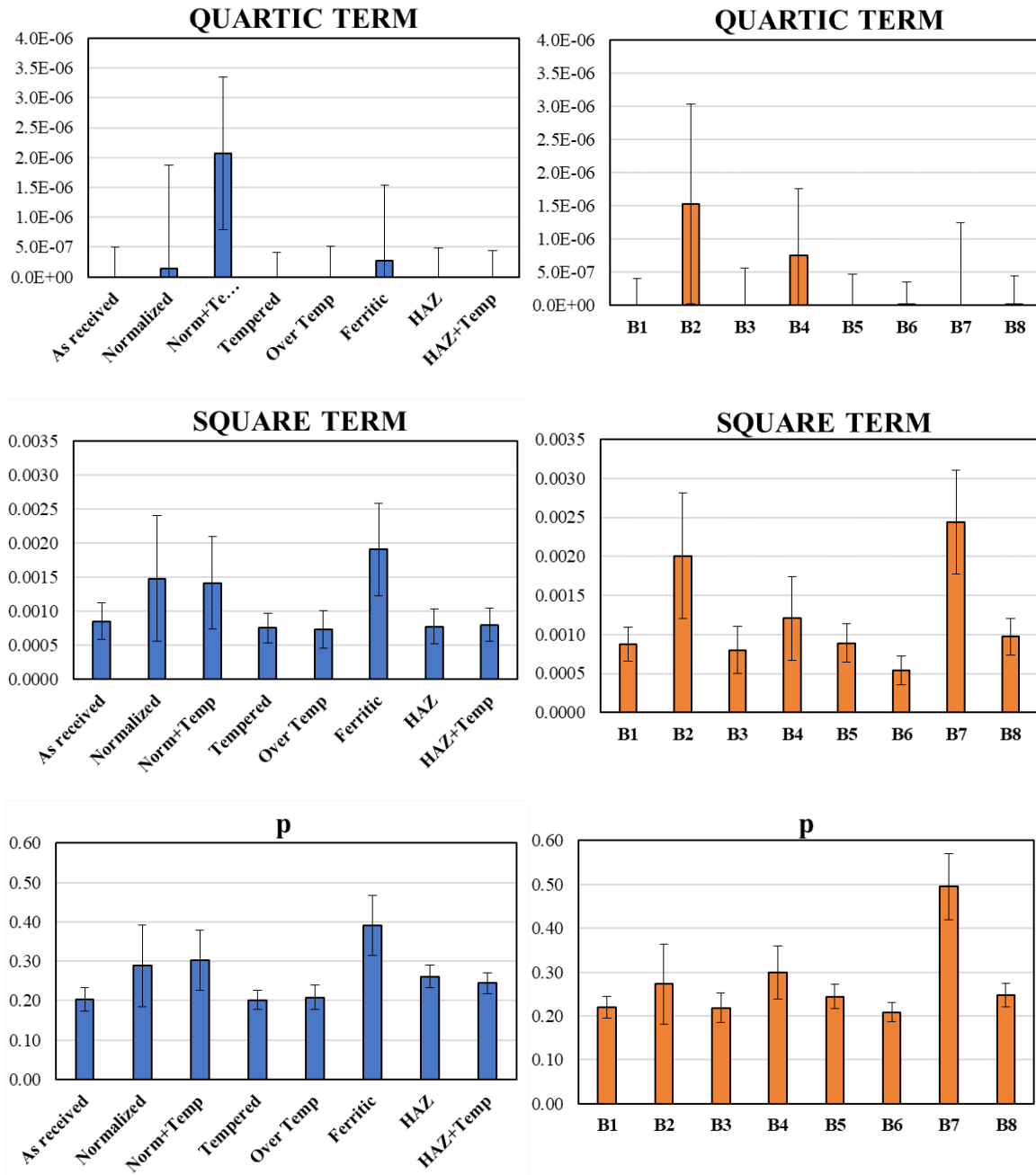


Fig. 14: Curve fitting coefficients for the known and blind TUBE samples.

These results suggest that there are two groups of samples, i.e. 1. Normalized, normalized+tempered, ferritic, and 2. Rest of the samples. This observation is consistent in both the known and unknown samples.

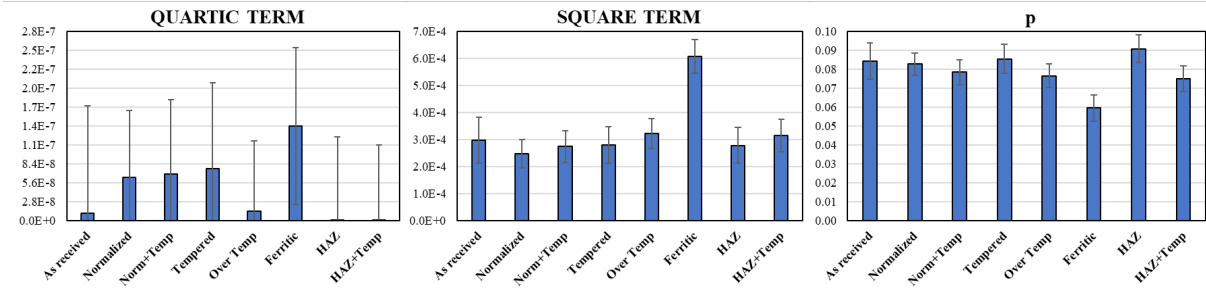


Fig. 15: Curve fitting coefficients for the PIPE-SECTIONS.

The Ferritic pipe-section stands out in both quartic and quadratic terms.

4.2. Backscatter term

The backscatter results are not as clear as the attenuation terms. However, some observations can be made for the tubes: the backscatter is slightly higher for Normalized, Normalized+tempered, Over tempered and HAZ+tempered. However, ferritic response is similar to as received. In the blind set of samples, three samples stand out compared to the others, B2, B7 and B8.

4.3. Absorption:

The absorption measurements for the tubes also show 2 groups similar to attenuation results; the ferritic and normalized samples have a higher absorption compared to rest of the samples. The "As Received" sample has the lowest absorption of the entire set. The blind set of samples show that there are 3 samples which stand out from the rest: B2, B4 and B7.

For the pipe cross-sections and whole pipe sections, such a clear distinction between samples or groups of samples could not be made, as the relative differences in Q^{-1} were not as prominent as in the tubes.

There was no noticeable difference in the values of Q^{-1} considering the polished and unpolished regions separately – indicating that the measurement is independent of the surface condition. Details of this is shown in Appendix 5.

4.4. Comparison between known and blind tube samples

Based on the above results, a few observations can be made: the following grouping can be seen.

1. Attenuation coefficient:
 - a. Parameter A: Normalized+Tempered, Ferritic, and Normalized, and B2 and B4.
 - b. Parameter B: Ferritic, Normalized, Normalized+tempered, and B2, B4 and B7.
2. Backscatter term: Normalized, Normalized+tempered, Over tempered, and HAZ+tempered, and B7, B8, B2.
3. Absorption: Ferritic and Normalized, and B2, B4 and B7.
4. We can also make an additional comparison between the data sets; compare parameter B with absorption results. We can observe that ferritic and normalized are higher than the rest in both B and absorption. Similarly, B2, B4 and B7 are once again grouping in both B and absorption.

These results point to the idea that we can distinguish between two sets of samples: in the known batch: normalized, normalized+tempered and ferritic, and rest of the samples. In the blind batch: B2, B4, B7 and rest of the samples. Exactly identifying which sample corresponds to which is challenging from these results.

5. Concluding remarks

We can make a few observations from the results from the ultrasonics characterization study:

1. The microstructure of all samples is less attenuative than conventional cold rolled samples, which points towards a small grain size. This is also the reason why we had to use 30MHz transducers to observe the difference between them.
2. However, the use of 30MHz transducer also meant that we will be more susceptible to surface variations. This is reflective of the data set reduction from 7000 points to 3000 points for attenuation and backscatter measurements.
3. The results do not show a clear difference between each sample. However, they show grouping, i.e. few samples are different compared to the others.
4. Final identification using these results show that we can distinguish two groups: In the known batch: normalized, normalized+tempered and ferritic, and rest of the samples. In the blind batch: B2, B4, B7 and rest of the samples.

APPENDIX 1: PRELIMINARY RESULTS ON STANDARD SAMPLES

To validate the setup and measurement method, we started by measuring the attenuation coefficient of a standard stainless-steel bar. The attenuation coefficient as a function of frequency has a power law trend, with the coefficient typically between 1-4. The measurement was done using front wall and backwall1 and backwall 1 and 2, which will be explained in Appendix 3. The results are shown in Fig. A1.1.

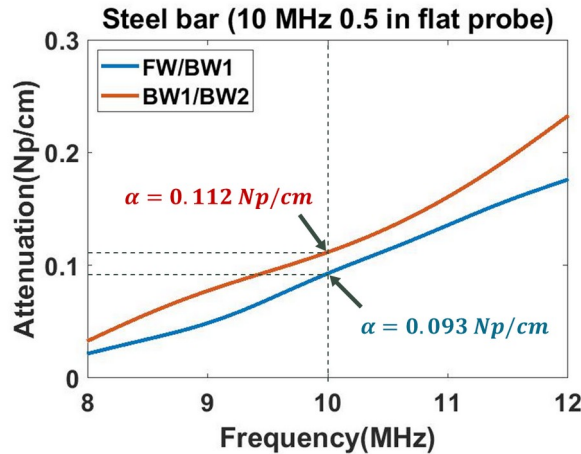


Figure A1.1. Attenuation as function of frequency of a steel bar of 0.5 in of thickness.

Both curves showed a similar trend. The values are similar to reported ultrasonic attenuation coefficient values for steel

APPENDIX 2: PIPE-CROSS SECTION CHARACTERIZATION

The same technique was applied to pipe cross section samples. This step was determine to the frequency and transducer diameter combination which will best serve us.

The pipe cross-sections were tested on their flat surfaces to obtain the attenuation coefficient and a backscatter term. Each specimen was tested in two points (2 and 3). Also, C-scans of these samples are presented.



Fig. A2.1: The pipe cross section samples used for testing.

We measured the attenuation coefficient at three different points (as shown in Fig. A2.1), using 5, 10, 20, and 30 MHz transducers. The results for 10MHz transducers are shown in Fig. A2.2, and A2.3. The results from point 1 were discarded since the proximity of this point to the square holes affected the results. We can notice that the curve is flat and does not show a power law dependence, which suggested that the frequency range of operation is small. So, we chose to increase the frequency up to 30 MHz in our main measurements.

The velocities, attenuation coefficient and backscatter term measured for these samples are shown in Table A2.1.

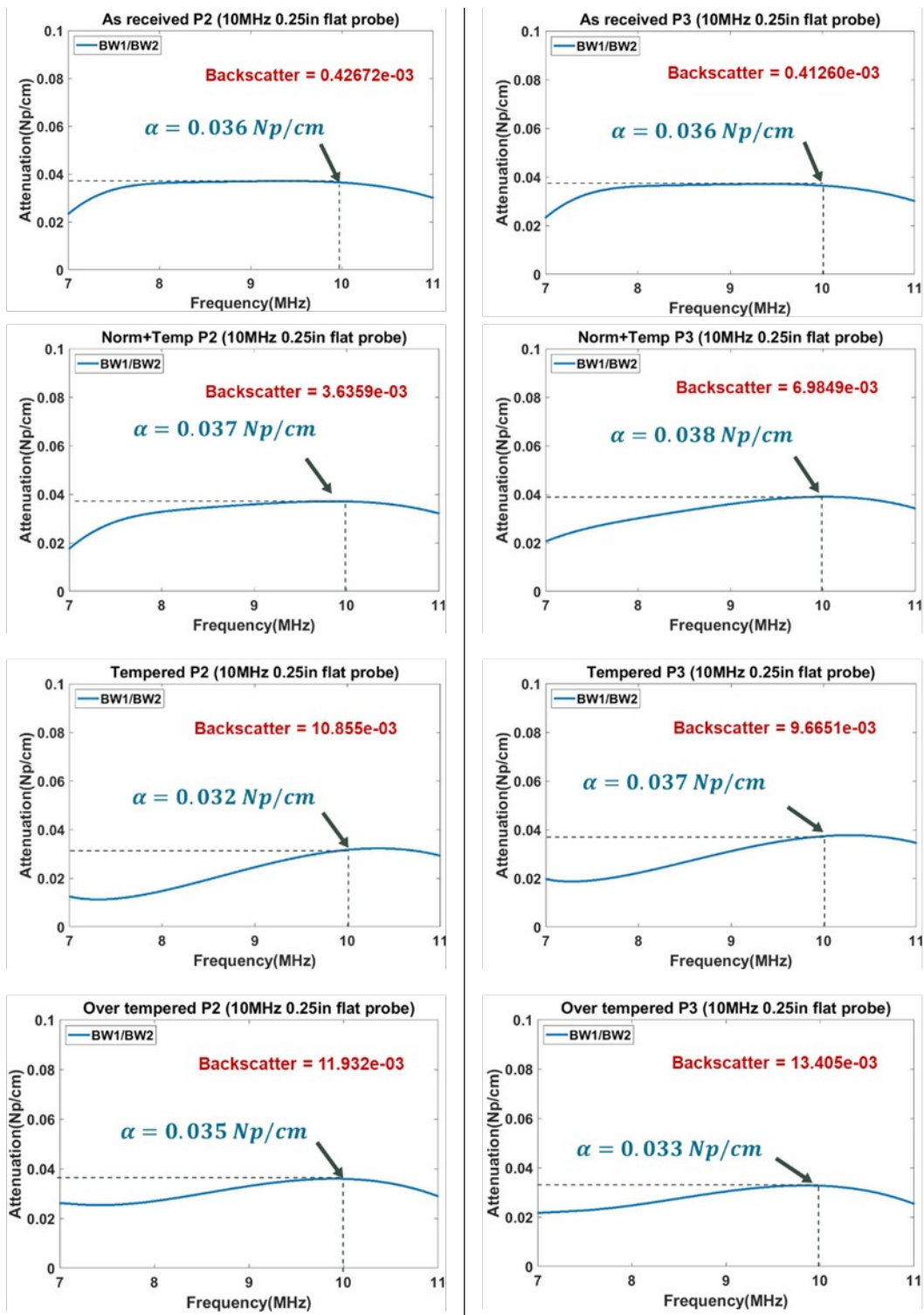


Fig. A2.2: Attenuation coefficient for various samples at two points P2, P3 at 10MHz.

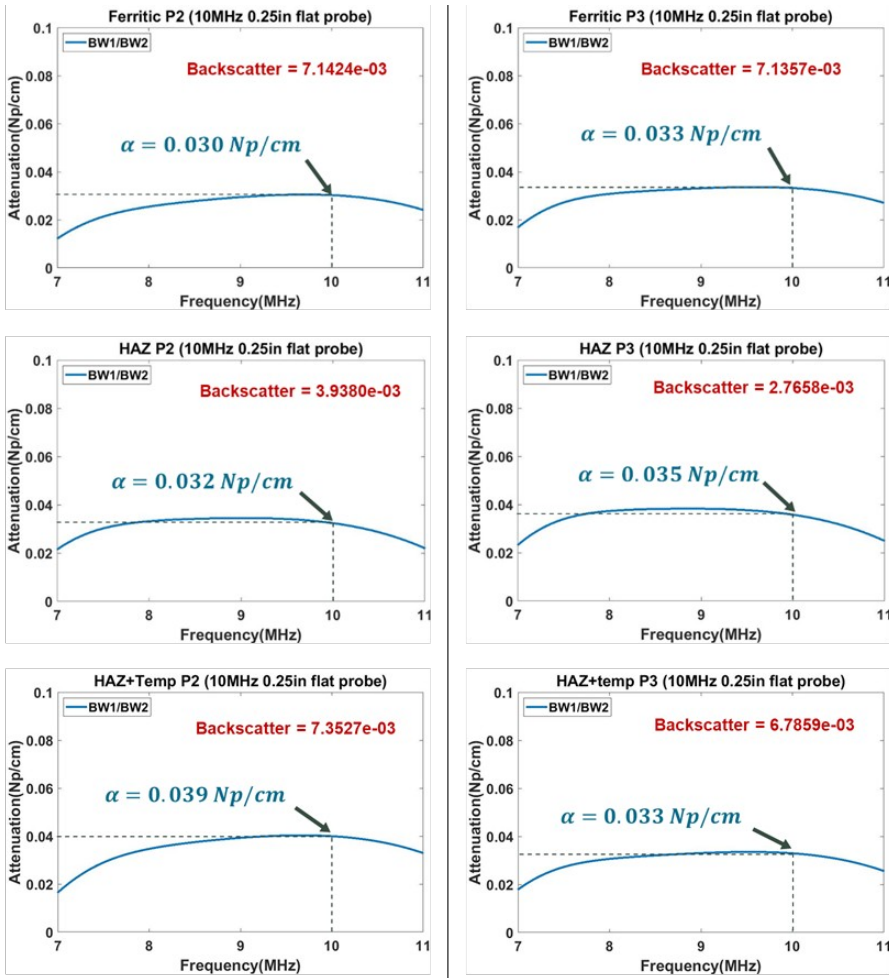


Fig. A2.3: Attenuation coefficient for various samples at two points P2, P3 at 10MHz.

Table A2.1. Pipe cross-section specimens: velocity, attenuation and backscatter term (t)

| SAMPLE | THICKNESS (mm) | Longitudinal velocity (m/s) | ATTENUATION (Np/cm) | BACKSCATTER (RMS) |
|-----------------|-------------------|-----------------------------|---------------------|------------------------|
| As received | 9.694 ± 0.007 | 5944 ± 11 | 0.036 | 0.42×10^{-3} |
| Norm + Tempered | 9.613 ± 0.013 | 5941 ± 5 | 0.037 | 5.31×10^{-3} |
| Tempered | 8.719 ± 0.029 | 5948 ± 5 | 0.035 | 10.26×10^{-3} |
| Over Tempered | 8.956 ± 0.020 | 5950 ± 2 | 0.034 | 12.66×10^{-3} |
| Ferritic | 9.919 ± 0.033 | 5895 ± 6 | 0.032 | 7.14×10^{-3} |
| HAZ | 9.011 ± 0.012 | 5896 ± 4 | 0.033 | 3.35×10^{-3} |
| HAZ + Tempered | 9.290 ± 0.016 | 5941 ± 2 | 0.036 | 7.07×10^{-3} |

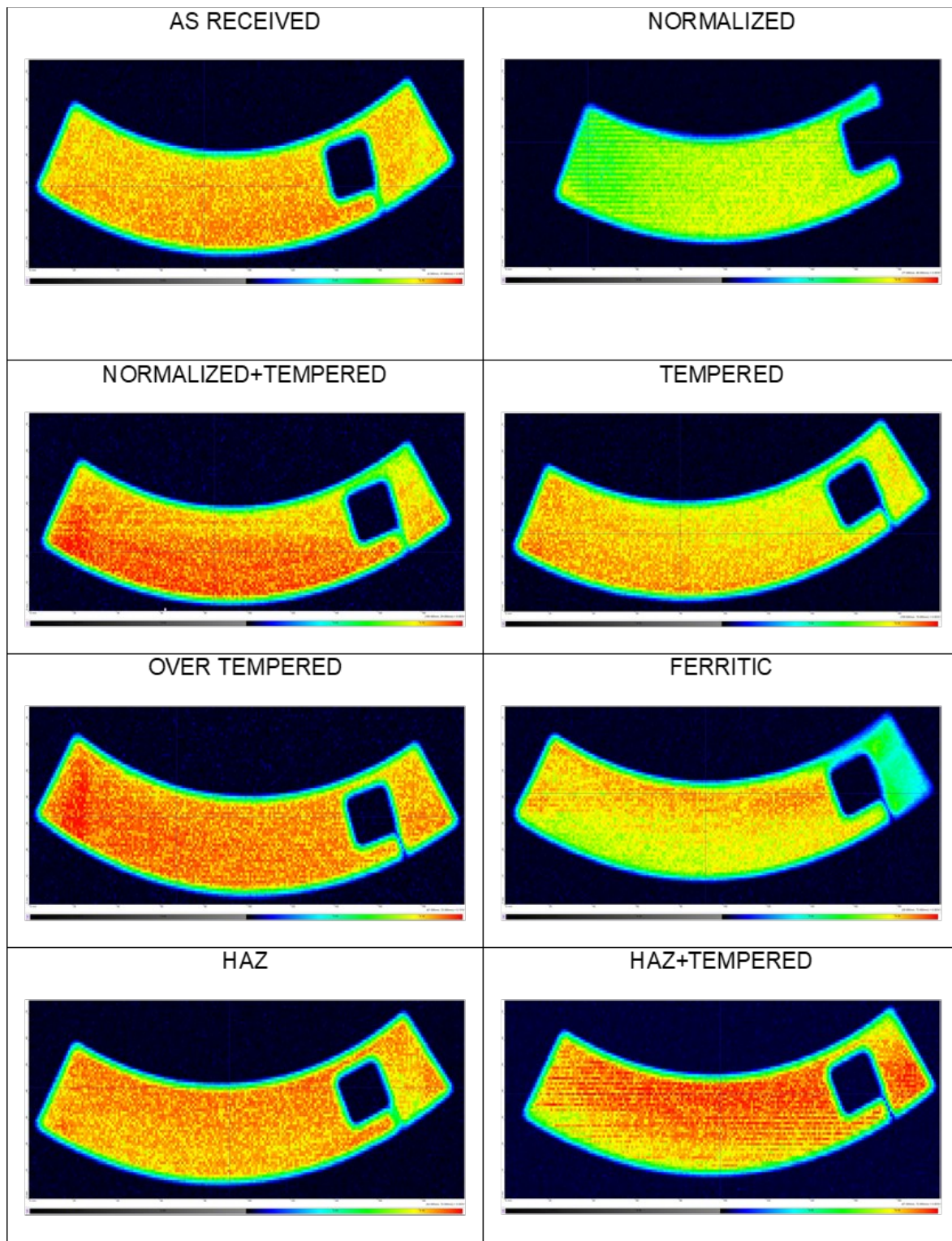


Fig. A2.4: Amplitude C-Scan of the cross sections.

APPENDIX 3: DETAILS OF ALPHA MEASUREMENT AND LINESCAN

When an elastic wave travels through a metallic sample, it interacts with the microstructural features of this sample. The acoustic energy is affected by these interactions, therefore, the quantification of this reduction of acoustic energy as a function of frequency provides information about the microstructure of a sample.

All the experiments to determine the attenuation and backscatter were done in immersion and the preliminary experiments were performed with a setup as the one shown in Fig A3.1. The experiments with the tubes are shown in Figure A3.2. The principle to determine the attenuation and backscatter is the same for all experiments, following the development explained next.

The ultrasonic immersion transducer is placed at a position where its face is in contact with water, the transducer sends an ultrasonic wave that travels through water, when the wave reaches the interface water-specimen, part of the acoustic energy is reflected back to the transducer as echo A (front-wall) and part of the energy is transmitted to the specimen, this transmitted wave reaches the bottom of the specimen and reflects from the interface specimen-water, it travels back transmitting again through the top of the specimen and then reaching the transducer as echo B (first back-wall). Part of the energy that was not transmitted into the water reflects from the interface at the top of the specimen and travels to the bottom, then it reflects at that interface and, similarly as with echo B, travels back to the transducer as echo C (second back-wall).

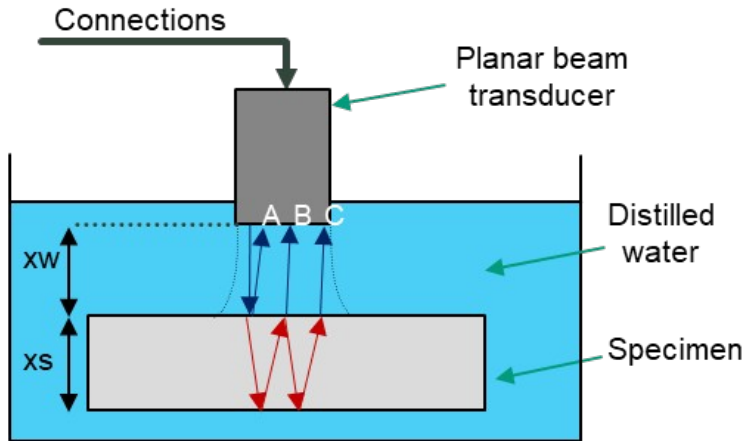


Figure A3.1. Immersion setup where the specimen is inside of a water tank filled with distilled water.

A waveform in time-domain containing the 3 echoes A, B and C or front-wall, first back-wall and second back-wall, respectively, is collected. From this waveform, the attenuation and the backscatter parameters are determined.

The amplitude of each echo is expressed as it follows:

$$A = FW = A_0 * e^{-2\alpha_w x_w} * R_{ws} * D(s_{FW})$$

$$B = BW1 = A_0 * e^{-2\alpha_w x_w} * T_{ws} * R_{sw} * T_{sw} * e^{-2\alpha_s x_s} * D(s_{BW1})$$

$$C = BW2 = A_0 * e^{-2\alpha_w x_w} * T_{ws} * T_{sw} * R_{sw}^3 * e^{-4\alpha_s x_s} * D(s_{BW2})$$

Where:

- FW , $BW\ 1$ and $BW\ 2$ are the amplitudes of the front-wall, 1st back-wall and 2nd back-wall echoes, respectively.
- A_0 is the initial amplitude of the wave coming from the transducer.
- α_w and α_s are the attenuation coefficients of the water and the specimen, respectively.
- x_w and x_s are the water path and the thickness of the specimen, respectively.
- R_{ws} , R_{sw} , T_{ws} , T_{sw} are the reflection and transmission coefficients at the interface water-specimen and specimen-water.
- $D(s_{FW})$, $D(s_{BW1})$, $D(s_{BW2})$ are the Lommel-Diffraction corrections:

$$D(s) = 1 - e^{-(\frac{2\pi i}{s})} \left[J_0\left(\frac{2\pi}{s}\right) + i J_1\left(\frac{2\pi}{s}\right) \right]; \quad s = \frac{4\pi z}{ka^2}$$

- z is the propagation distance.
- a is the transducer radius.
- k is the wavenumber.

Finally, taking the amplitude ratio between consecutive echoes, we obtain two equations to determine the attenuation coefficient:

$$\alpha_s = \frac{1}{2x_s} \ln \left(\left| \frac{FW(f)}{BW\ 1(f)} \right| * (R_{sw}^2 - 1) * \left| \frac{D(s_{BW1})}{D(s_{FW})} \right| \right) \dots (\text{Eq. 1})$$

$$\alpha_s = \frac{1}{2x_s} \ln \left(\left| \frac{BW\ 1(f)}{BW\ 2(f)} \right| * R_{sw}^2 * \left| \frac{D(s_{BW2})}{D(s_{BW1})} \right| \right) \dots (\text{Eq. 2})$$

The experiments with the tubes were done with a setup shown in Figure 2. As the tubes have a curved surface, the diffraction correction of equations 1 and 2 are not applicable, this correction was not considered for the results presented in this report. These results were obtained using equation 3.

$$\alpha_s = \frac{1}{2x_s} \ln \left(\left| \frac{BW\ 1(f)}{BW\ 2(f)} \right| * R_{sw}^2 \right) \dots (\text{Eq. 3})$$

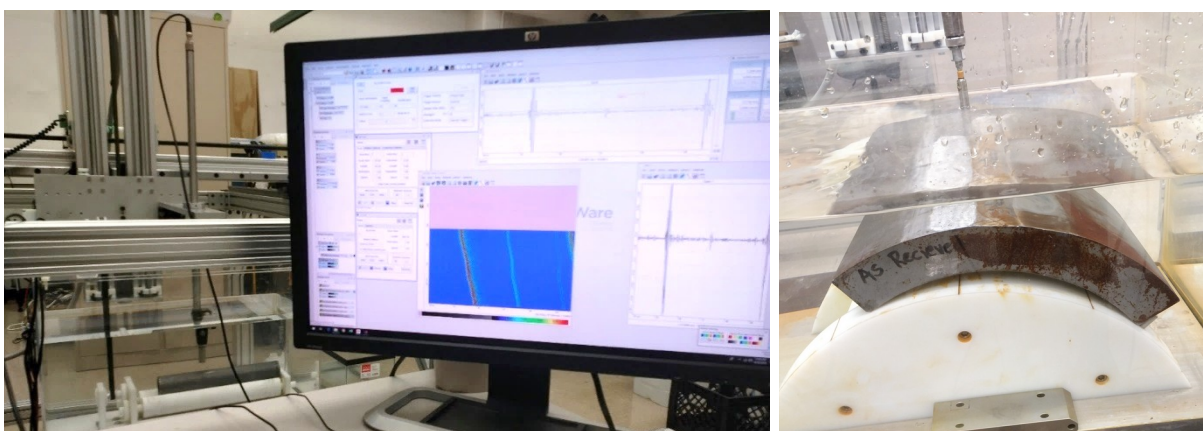


Figure A3.2. Immersion setup for the attenuation and backscatter experiments with the tubes and pipe-sections.

The ultrasonic attenuation coefficient was determined for the 16 tubes and 8 pipe-sections. This experiment was realized with an immersion setup (See figures 1 & 2).

For the tubes, the pulse was generated with a pulser (Panametrics 5601A). A flat surface ultrasonic immersion transducer of 30 MHz and nominal element size diameter of 0.25 in (Olympus V356-SU) was utilized for all these experiments. This ultrasonic transducer has a delay fused silica. For the pipe-sections, the setup consisted of a pulser (Panametrics 5055PR) and a flat immersion transducer of 20 MHz and 0.25 in element size (Olympus V317-SM).



Figure A3.3. Tubes marked each 30°. Pipe-section with some polished regions.

The data collected consisted of linescans at 12 different angles per tube increasing each 30°, for the pipe-sections, 8 linescans were collected in different regions (~4 non-polished and ~4 polished). In each linescan, the transducer was normalized at the central axis of the sample and to cover the whole length of the samples, 300 mm were scanned for the tubes and 230 mm for the pipe-sections. A typical linescan is shown in figure A3.5.

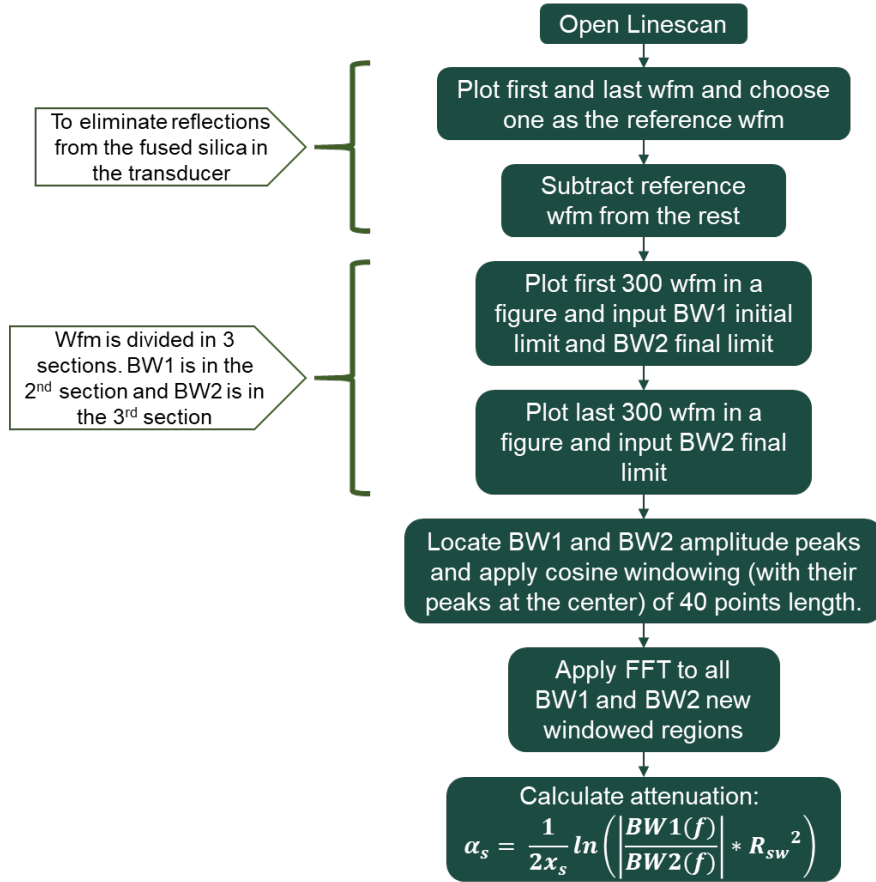


Figure A3.4. Flowchart of the processing in MATLAB to determine the attenuation coefficient per scan position.

The horizontal axis of the linescan shows the time-of-flight (TOF) and the vertical axis shows the position along the tube from 0 to 300 mm. Each horizontal line at a specific vertical position represents a waveform at that position.

As it can be observed, the TOF of the echoes varies along the linescan. This is explained due to the variation of thickness of the tube along its axis and because ultrasonic testing is tremendously sensitive to these variations. Another characteristic of these linescans is the presence of blue vertical lines. These blue lines correspond to reflections from the fused silica disk and they arrive at the same time for each waveform and have the same amplitude and phase along the linescan since there is no variation of thickness in this fused silica disk.

The processing to calculate the attenuation coefficient is summarized in the flowchart of Fig. A3.4. In order to determine the attenuation coefficient at each scanning position, a preliminary step had to be applied to the processing. This step consisted in removing the reflections from the silica disk inside the ultrasonic transducer from each waveform. As each linescan contains 300 mm of data, either the initial or last collected waveform per linescan was defined as the reference waveform and then this waveform was subtracted from the rest of the waveforms. The criteria to select the initial or final waveform depended on if the initial waveform had not carried information from the sample (which happened in a few cases), in that case the final waveform was selected as the reference waveform.

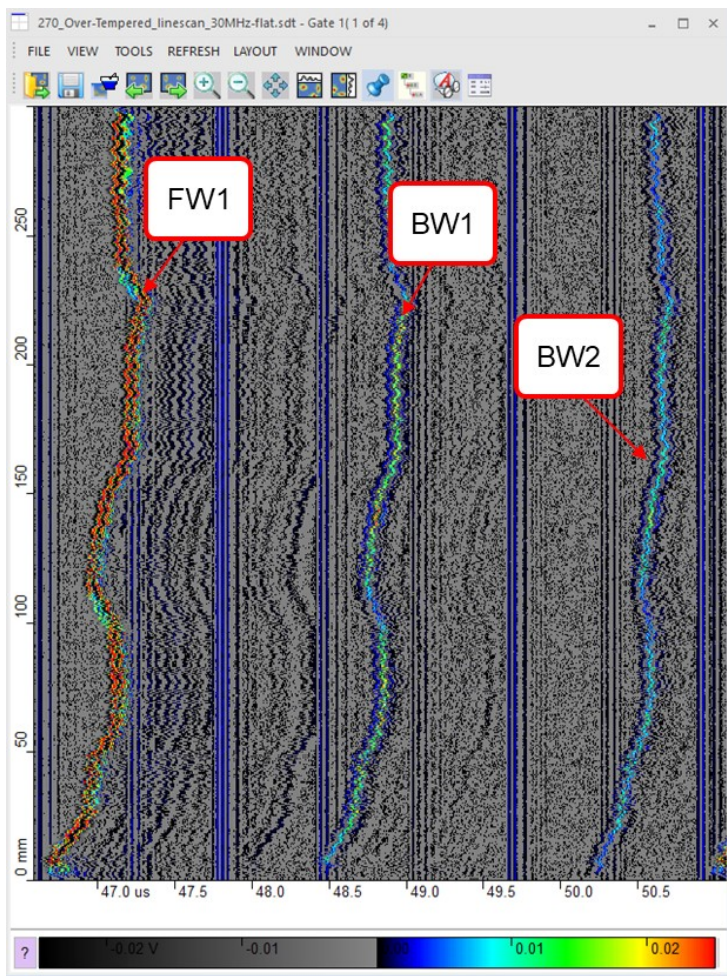


Figure A3.5. Linescan of the Over-tempered tube at 270°.

The MATLAB code to determine the attenuation coefficient per position contains the aforementioned processing step. Both the initial and last waveform are plotted in the same figure and the user has the power to decide which waveform is utilized as a reference.

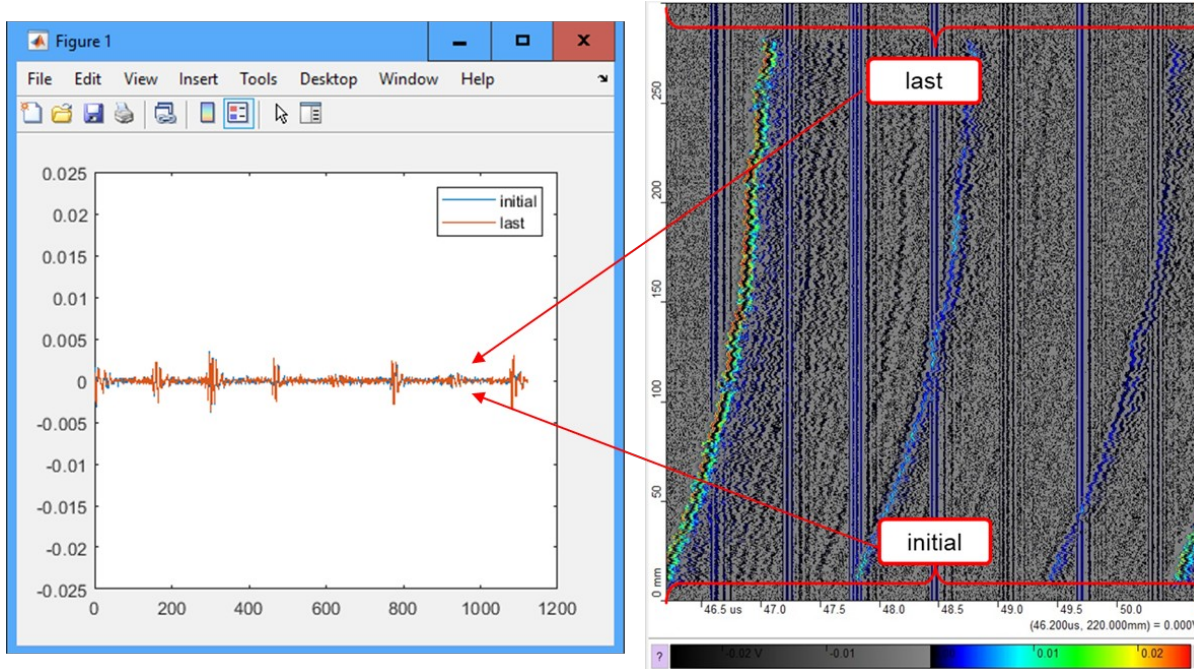


Figure A3.6. Initial and last waveforms of the “Normalized+Tempered” tube at 0° are plotted.

The next step of the processing consisted in applying window functions to separate each echo in the waveforms since only BW1 and BW2 echoes were required in order to determine the ultrasonic attenuation parameter.

The initial idea consisted in dividing the waveform in 3 regions and then find the maximum amplitude in each region, which ideally would result in FW, BW1 and BW2. However, due to thickness variation along the axis of the tubes for some angles, sometimes a second front-wall (FW2) reflection came into picture and therefore, that echo has the maximum amplitude in the third region of the waveform. After observing each linescan, we noticed that in the cases where a FW2 echo was appearing, this echo only appeared in the first half of the scanned positions, in other words, this issue would only be possible from 0 to 150 mm of the linescan which consist in 300 scanned positions (each linescan consisted of 600 waveforms).

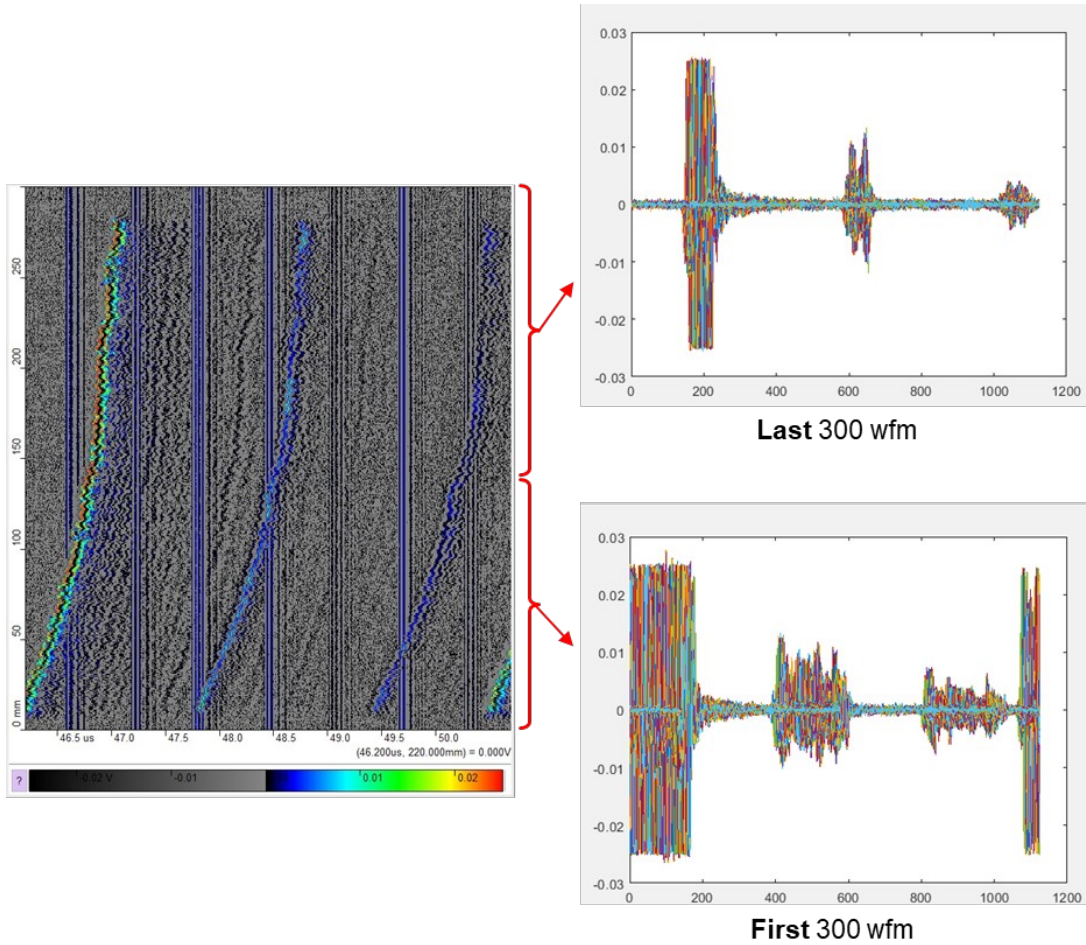


Figure A3.7. Waveforms of the Normalized+Tempered tube at 0° were plotted.

The implementation of this step in the code consisted in plotting the first 300 waveforms of the linescan and the user defines the window ranges for BW1 and BW2 were the code should search for a maximum amplitude. Then, plotting the last 300 waveforms and repeat the same criteria (see Figure A3.7). This step was performed after removing the vertical blue lines from the linescan.

Finally, the last step of the processing consisted on applying windows to separate the BW echoes (following the previous step). Each window consisted of 40 sample points with the maximum amplitude value in the center of the window. Thus, from each linescan 600 BW1 and 600 BW2 echoes were obtained and from the frequency spectrum was computed for each of these echoes using the FFT command in MATLAB. The 600 BW1, BW2 and FFT of these echoes is shown in Figure A3.8.

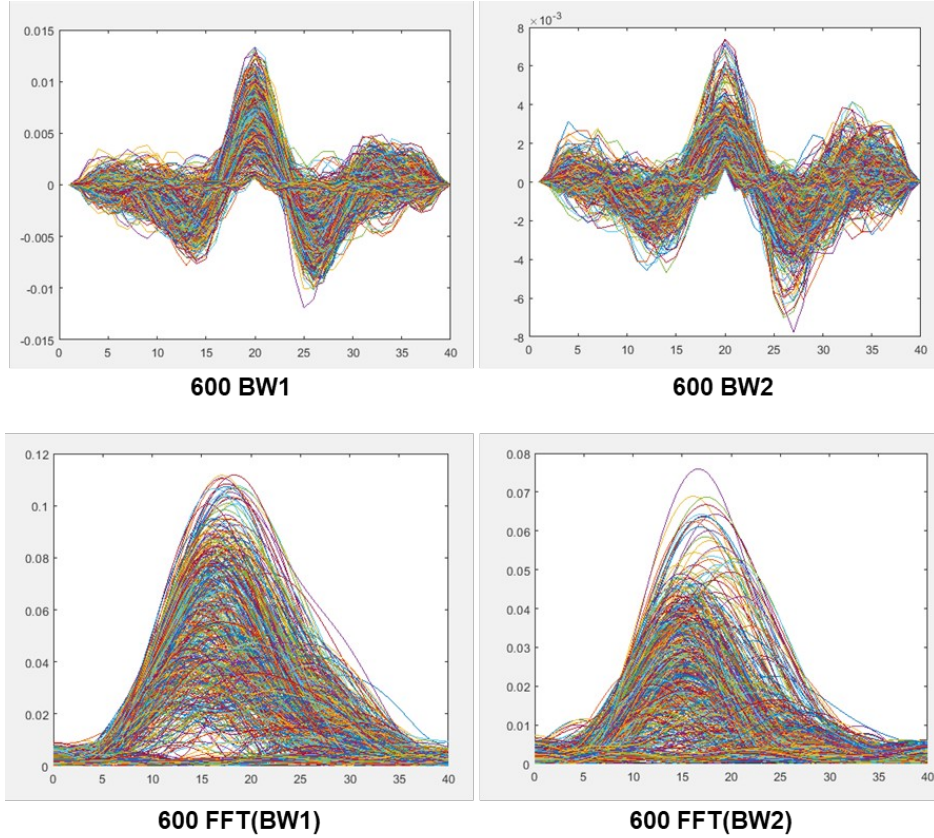


Figure A3.8. All BW1, BW2 echoes and their respective frequency spectrum are plotted.

Of course, some of the initial and last positions from the 600 scanned points do not contain any information from the tube. Therefore, that explains some “weird” frequency spectrum plots. Once the frequency spectrum for all the scanned positions is obtained, the ultrasonic attenuation coefficient can be determined for all points with equation 3:

$$\alpha_s = \frac{1}{2 x_s} \ln \left(\left| \frac{BW 1(f)}{BW 2(f)} \right| * R_{sw}^2 \right)$$

C-scans were generated with all the processed data for the 16 tubes (7200 scan points) and 8 pipe-sections (3680 scan points). The processed C-scans show lack of uniformity in all the results (attenuation and backscatter) per tube.

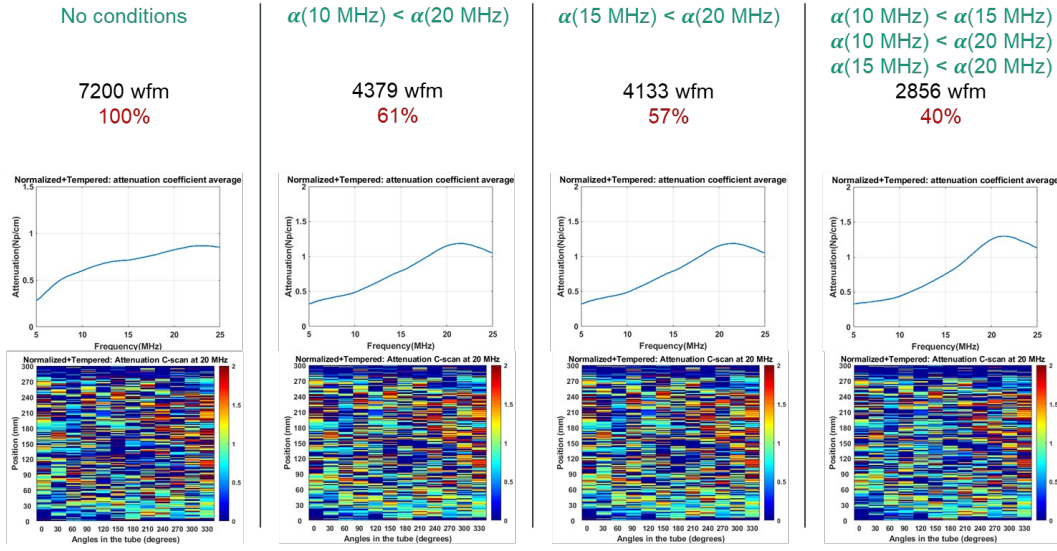


Figure A3.9. Conditions applied to consider "valid" datapoints.

For the case of the attenuation coefficient, some conditions were included in the code to remove “weird” data points. These “weird” data points occurred when in some scan positions where the tube was polished, the amplitude of BW2 appeared as greater than that of BW1, this was resulting in negative attenuation values. The attenuation coefficient generally follows an increasing trend with frequency and has positive values. Therefore, different conditions were applied to only consider datapoints where the amplitude of BW1 was greater than that of BW2 and where the attenuation at higher frequencies was greater than at lower frequencies (see Figure A3.9). In this way, new average attenuation curves per tube were determined with the condition:

$$\alpha(8 \text{ MHz}) < \alpha(12 \text{ MHz})$$

$$\alpha(12 \text{ MHz}) < \alpha(15 \text{ MHz})$$

$$\alpha(15 \text{ MHz}) < \alpha(18 \text{ MHz})$$

$$\alpha(18 \text{ MHz}) < \alpha(22 \text{ MHz})$$

Following these conditions, new datasets per tube were generated. A nonlinear fit following the model $\alpha = A f^4 + B f^2 + p$ was applied to determine the fitting parameters. This process was performed in MATLAB using the command lsqcurvefit (least squares fit) using as inputs the function that we were aiming to fit, the frequency (as a matrix) and the attenuation dataset per tube (also as a matrix). This process resulted in the parameters A, B and p for the fitted dataset.

The residual and jacobian were among the outputs of the lsqcurvefit function. With these two results, and using the nlpaci command and the fitting parameters, the confidence intervals (at 95% confidence) were obtained for each of the fitting parameters.

Furthermore, from the 95% confidence intervals, the standard deviation was calculated for each parameter and for each tube. The definition of the standard deviation is:

$$SD = SE \times \sqrt{N} \dots (\text{Eq. 4})$$

Where SE is the standard error and N is the dataset size (after the aforementioned conditions were applied). The standard error can be calculated from the confidence intervals, and in our case of 95% confidence and with dataset sizes bigger than 100, the SE is 3.92 standard errors wide. Thus:

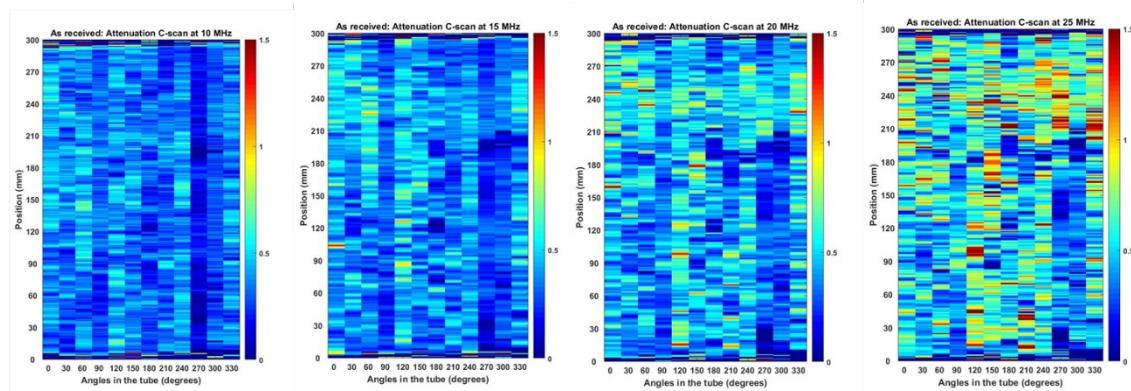
$$SD = \frac{(upper\ limit - lower\ limit)}{3.92} \times \sqrt{N} \dots (\text{Eq. 5})$$

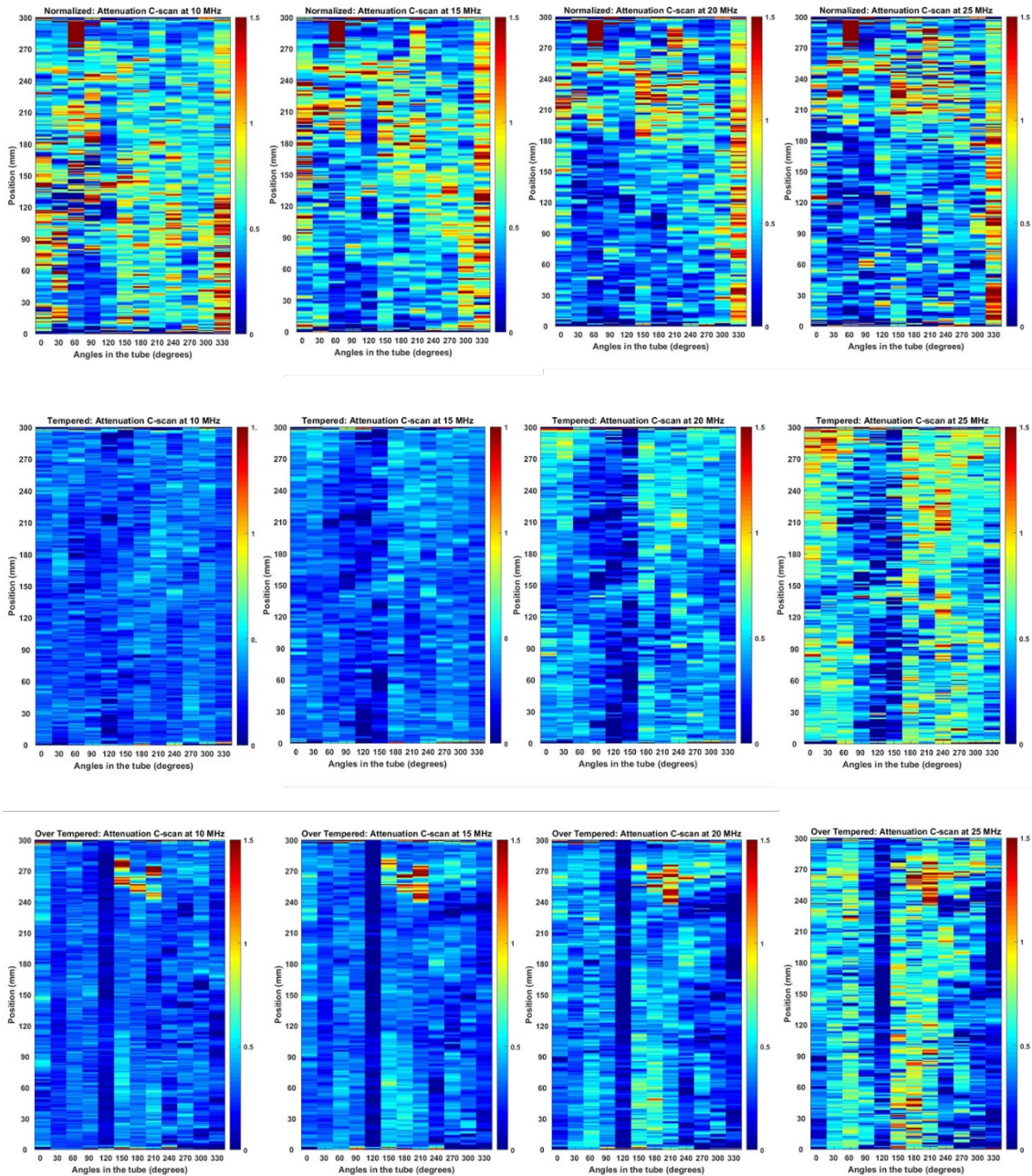
A3.1. ATTENUATION COEFFICIENT OF TUBE SAMPLES

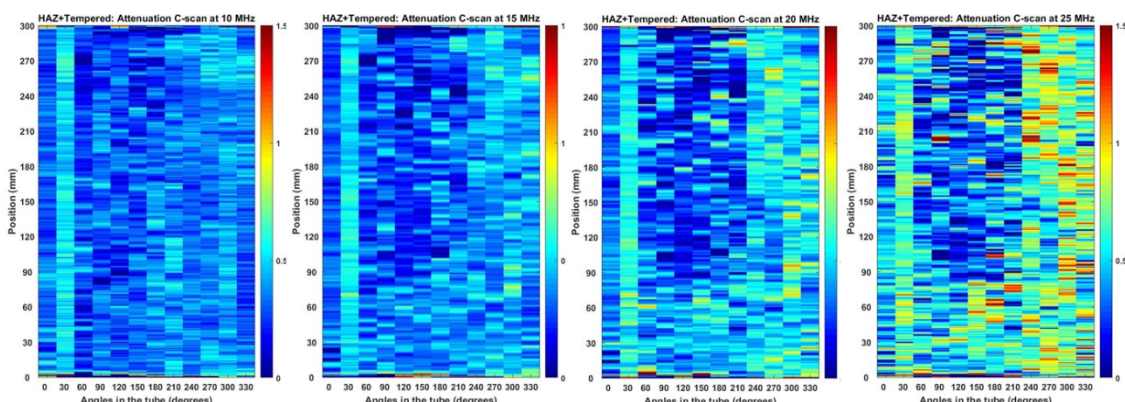
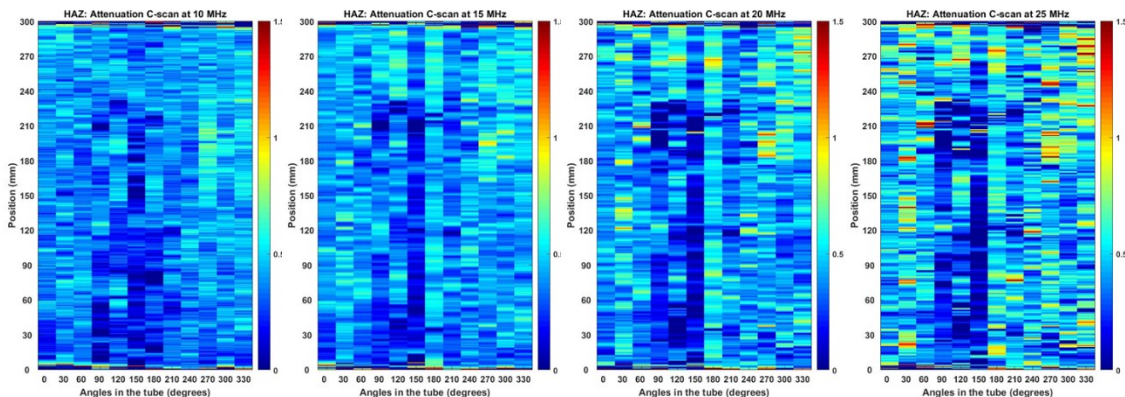
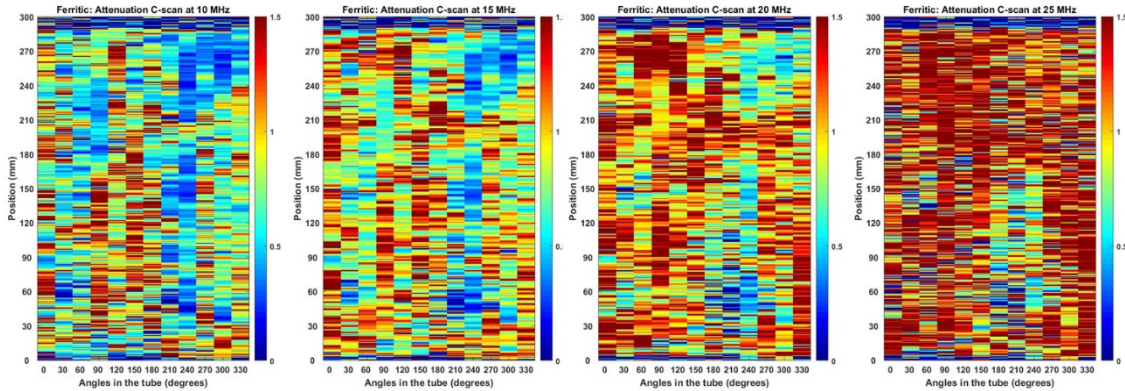
The attenuation fitting parameters and their standard deviations for the tubes are:

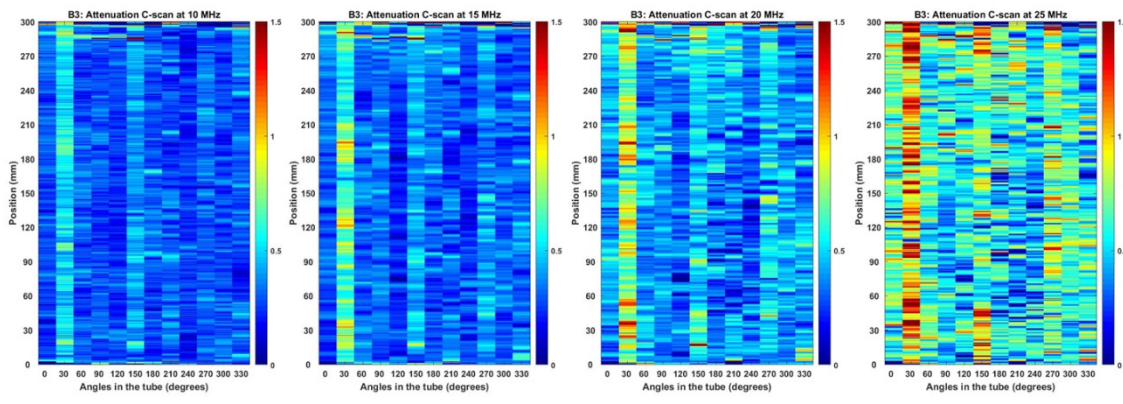
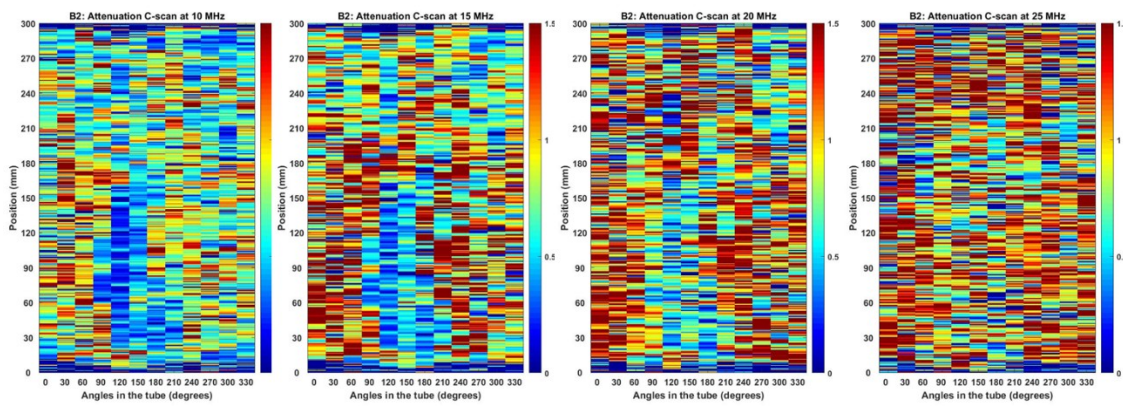
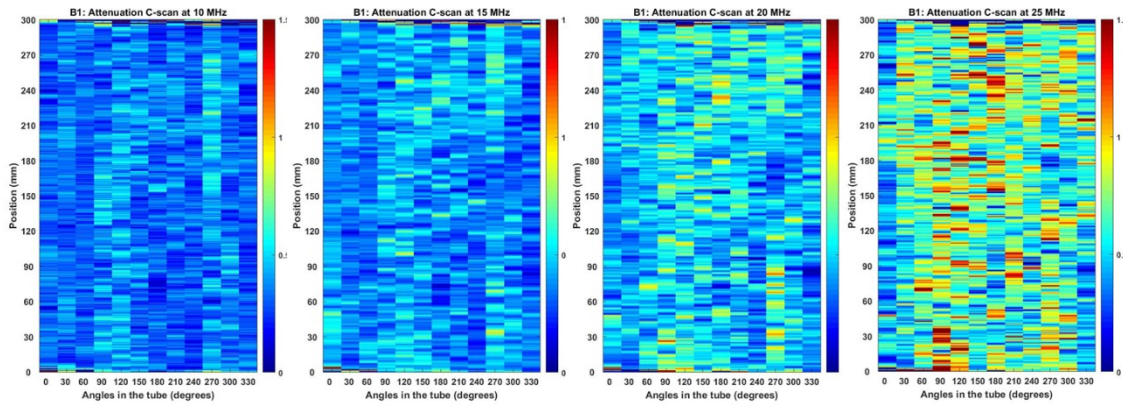
| TUBES | A | A std | B | B std | p | p std |
|--------------------|----------|----------|----------|----------|----------|----------|
| As received | 4.43E-13 | 5.06E-07 | 8.51E-04 | 2.70E-04 | 2.03E-01 | 3.05E-02 |
| Normalized | 1.44E-07 | 1.73E-06 | 1.48E-03 | 9.21E-04 | 2.88E-01 | 1.04E-01 |
| Norm+Temp | 2.07E-06 | 1.28E-06 | 1.41E-03 | 6.80E-04 | 3.02E-01 | 7.70E-02 |
| Tempered | 4.10E-13 | 4.06E-07 | 7.51E-04 | 2.17E-04 | 2.02E-01 | 2.45E-02 |
| Over Temp | 3.99E-13 | 5.10E-07 | 7.31E-04 | 2.72E-04 | 2.08E-01 | 3.08E-02 |
| Ferritic | 2.67E-07 | 1.27E-06 | 1.91E-03 | 6.78E-04 | 3.91E-01 | 7.67E-02 |
| HAZ | 4.04E-13 | 4.81E-07 | 7.72E-04 | 2.56E-04 | 2.62E-01 | 2.90E-02 |
| HAZ+Temp | 4.23E-13 | 4.47E-07 | 8.02E-04 | 2.38E-04 | 2.44E-01 | 2.69E-02 |
| B1 | 4.41E-13 | 4.09E-07 | 8.75E-04 | 2.18E-04 | 2.19E-01 | 2.47E-02 |
| B2 | 1.52E-06 | 1.51E-06 | 2.01E-03 | 8.02E-04 | 2.73E-01 | 9.08E-02 |
| B3 | 4.27E-13 | 5.64E-07 | 7.99E-04 | 3.00E-04 | 2.18E-01 | 3.40E-02 |
| B4 | 7.58E-07 | 1.00E-06 | 1.21E-03 | 5.35E-04 | 2.99E-01 | 6.05E-02 |
| B5 | 3.97E-13 | 4.67E-07 | 8.90E-04 | 2.49E-04 | 2.45E-01 | 2.82E-02 |
| B6 | 1.35E-12 | 3.50E-07 | 5.41E-04 | 1.87E-04 | 2.09E-01 | 2.11E-02 |
| B7 | 4.82E-13 | 1.25E-06 | 2.44E-03 | 6.65E-04 | 4.95E-01 | 7.52E-02 |
| B8 | 4.42E-12 | 4.41E-07 | 9.72E-04 | 2.35E-04 | 2.47E-01 | 2.66E-02 |

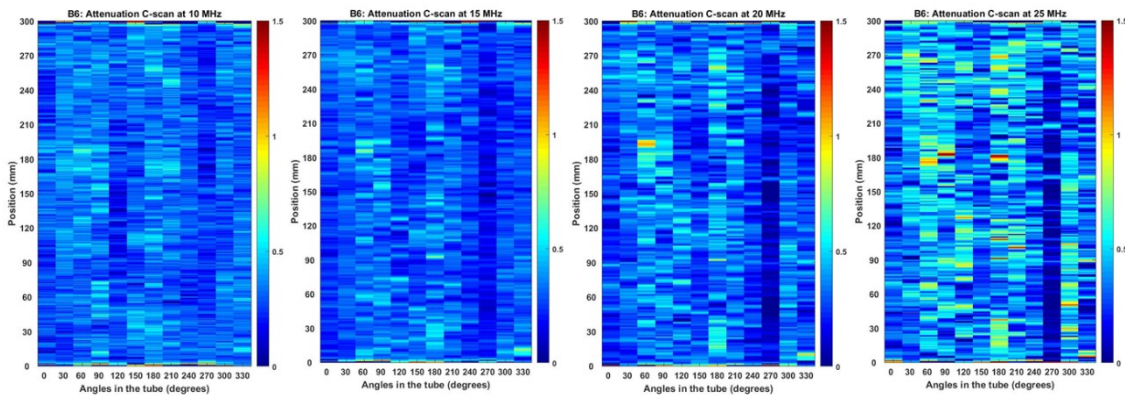
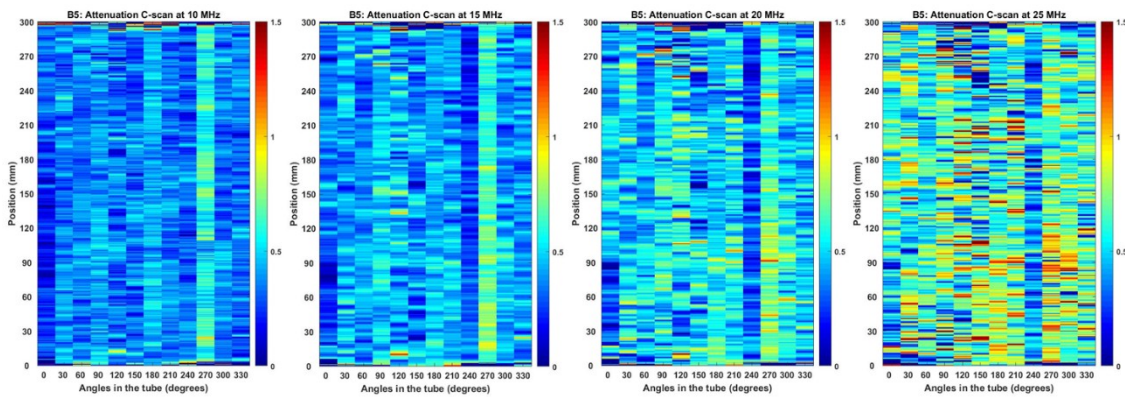
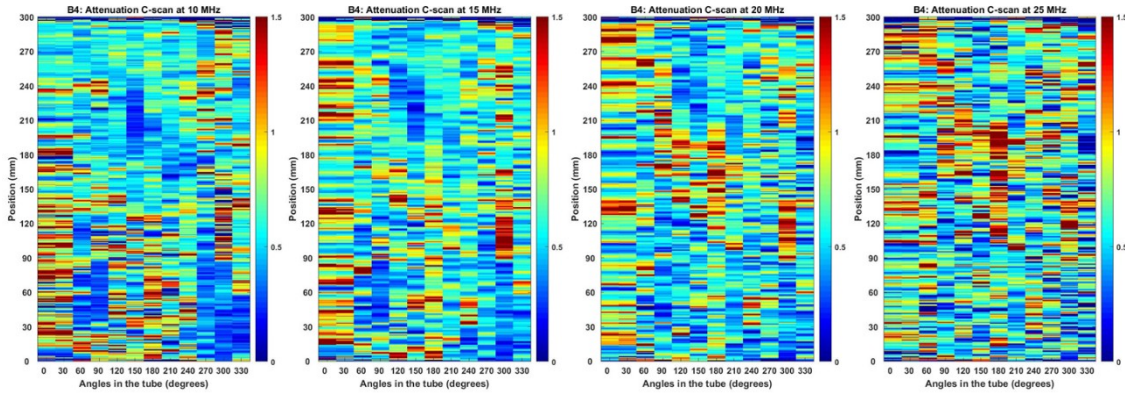
The following plots show the C-scans of the tubes with no conditions applied:

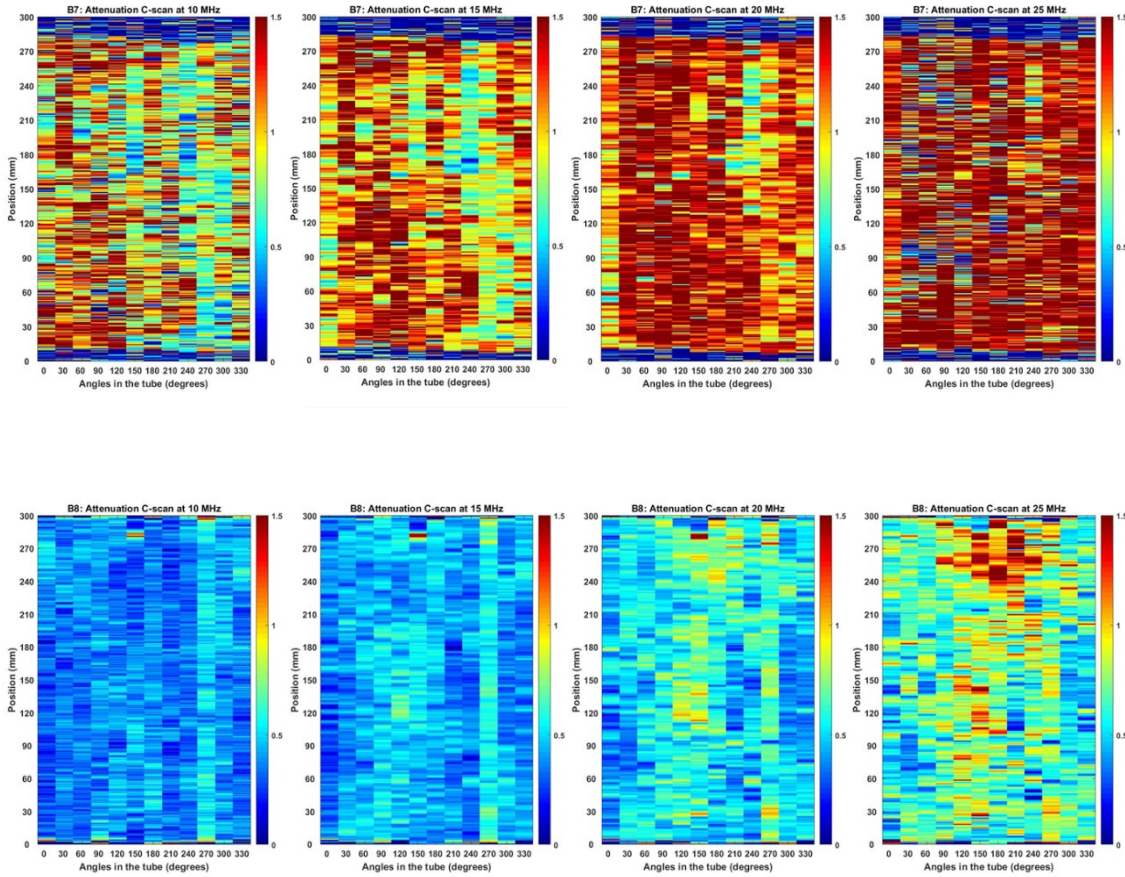










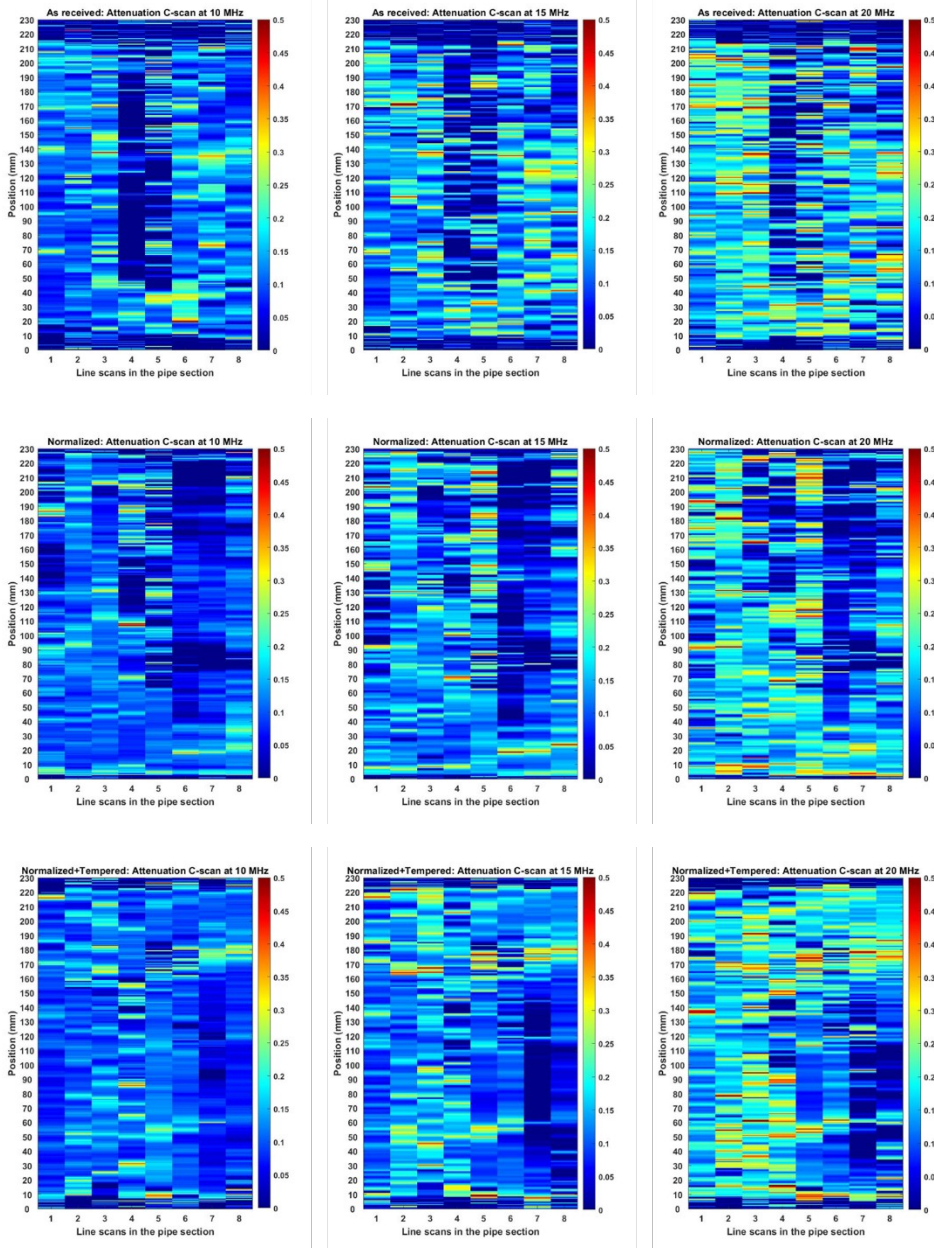


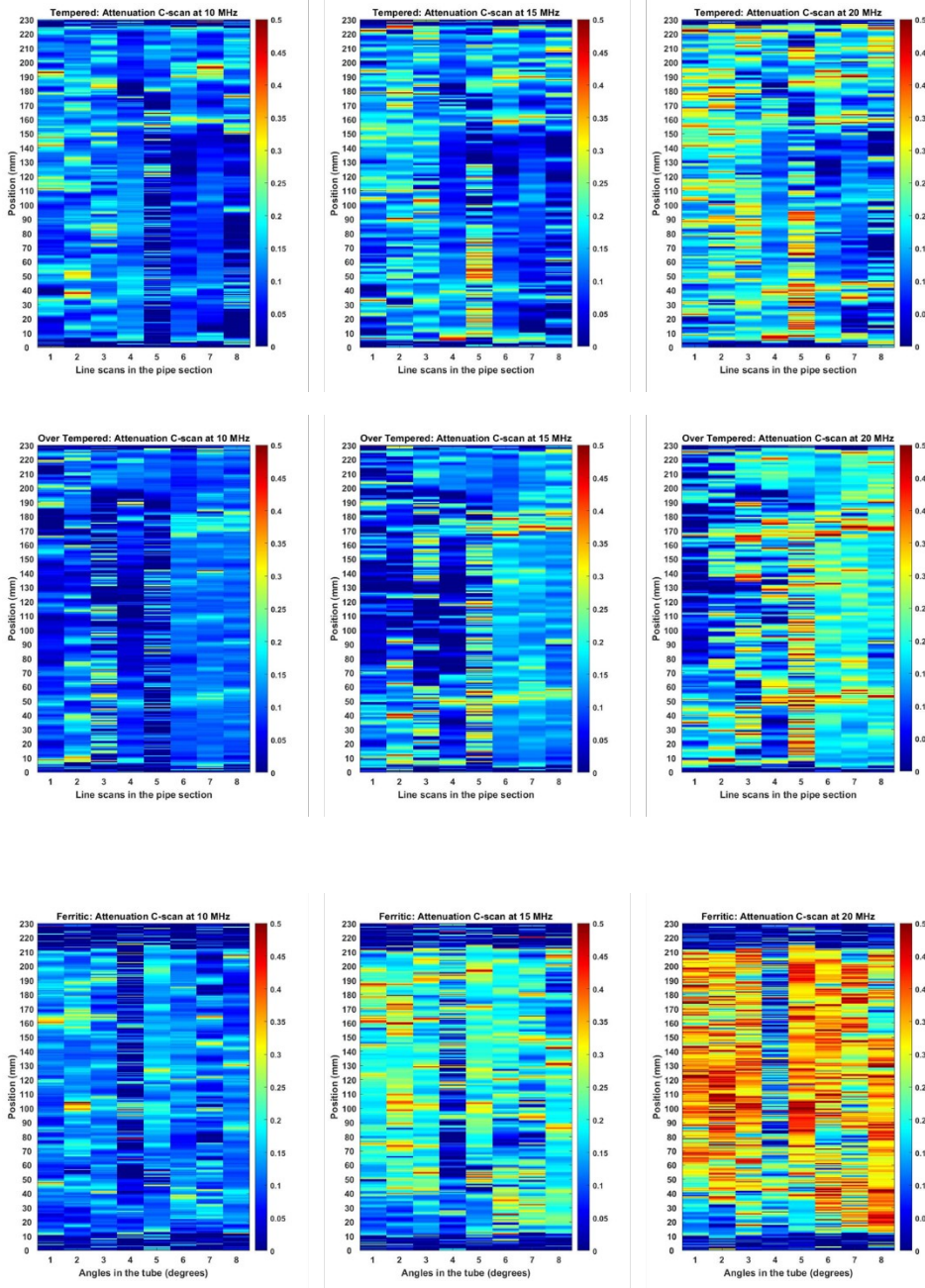
A3.2. ATTENUATION COEFFICIENT OF PIPE-SECTION SAMPLES

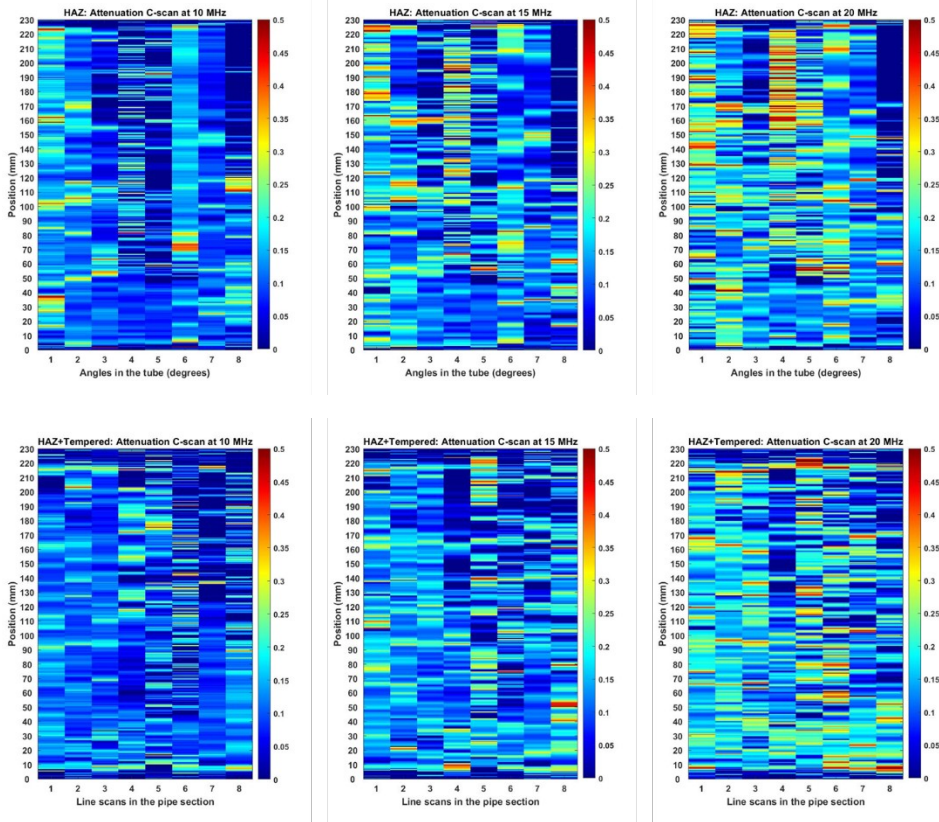
The attenuation fitting parameters and their standard deviations for the pipe-sections are:

| PIPE-SECTIONS | A | A std | B | B std | p | p std |
|--------------------|----------|----------|----------|----------|----------|----------|
| As received | 1.11E-08 | 1.59E-07 | 2.99E-04 | 8.47E-05 | 8.43E-02 | 9.57E-03 |
| Normalized | 6.43E-08 | 9.86E-08 | 2.49E-04 | 5.24E-05 | 8.27E-02 | 5.92E-03 |
| Norm+Temp | 6.88E-08 | 1.10E-07 | 2.74E-04 | 5.85E-05 | 7.85E-02 | 6.60E-03 |
| Tempered | 7.71E-08 | 1.27E-07 | 2.79E-04 | 6.74E-05 | 8.55E-02 | 7.61E-03 |
| Over Temp | 1.44E-08 | 1.04E-07 | 3.24E-04 | 5.52E-05 | 7.65E-02 | 6.24E-03 |
| Ferritic | 1.40E-07 | 1.16E-07 | 6.07E-04 | 6.17E-05 | 5.95E-02 | 6.97E-03 |
| HAZ | 2.26E-10 | 1.24E-07 | 2.78E-04 | 6.60E-05 | 9.09E-02 | 7.45E-03 |
| HAZ+Temp | 2.01E-13 | 1.12E-07 | 3.15E-04 | 5.95E-05 | 7.49E-02 | 6.72E-03 |

The generated C-scans are presented:







APPENDIX 4: DETAILS OF BACKSCATTER MEASUREMENT AND LINESCAN

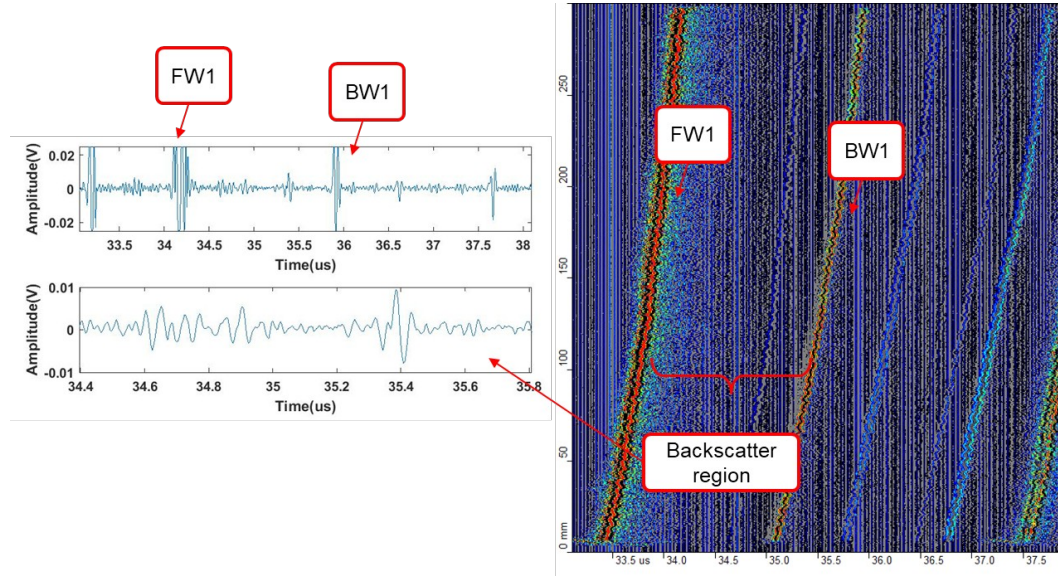


Figure A4.1. Linescan of the Over-tempered tube at 270° and waveform at the position 150 mm.

The ultrasonic backscatter coefficient was determined for the 16 tubes with the same setup used for the attenuation coefficient measurements. The only difference was the transducer. A focused ultrasonic immersion transducer of 30 MHz, diameter of 0.25 in and a focal length of 1.25 in (Olympus V376-SU) was utilized for all these experiments. Similarly, as with the flat immersion transducer, this ultrasonic transducer has a fused silica delay line between the active plate and the external surface. For the 8 pipe-sections, the same data collected to measure attenuation coefficient was used to determine the backscatter coefficient, the transducer used was a 20MHz-0.25in flat (Olympus V317-SM).

The water path was determined experimentally between the transducer vertical position that give the maximum amplitude of the front wall and the one that gives the maximum amplitude of the first back wall. With this step, the acoustic energy is focused on the backscatter region. The collection of data was the same as for the attenuation coefficient, 12 linescans per tube of 300 mm and 8 linescans per pipe-section of 230 mm.

The steps to calculate the backscatter coefficient start by windowing the backscatter region in time-domain and then applying the FFT to each of the datapoints, these steps are summarized in Fig. A4.2. Then, a spatial rms is applied to obtain the backscatter rms as function of frequency. This frequency dependent backscatter is further windowed to the transducer frequency bandwidth.

A reference signal of a fused silica sample with similar dimensional characteristics as the tested sample is required in order to obtain the final backscatter coefficient. The following equation determines the backscatter coefficient as a function of frequency when using a focused transducer:

$$\sqrt{\eta} = \frac{|\Gamma_{sample}(f)| |R_{w-FS}| a^2 \rho_w v_w |D_{FS}| k_s}{|\Gamma_{ref}(f)| 2 T_{ws}^2 \rho_s v_s e^{2\alpha_w x_w}} \left[\int_{-\infty}^{\infty} |C(f, x_1, y_1, z_1)|^4 P(z_1) e^{-4\alpha_s z_s} dx_1 dy_1 dz_1 \right]^{1/2} \dots \text{(Eq. 6)}$$

Where:

- η is the backscatter coefficient as a function of frequency.
- $|\Gamma_{sample}(f)|$ is the backscatter spatial RMS magnitude of the sample in frequency domain.
- $|\Gamma_{ref}(f)|$ is the fused silica reference echo magnitude in frequency domain.
- D_{FS} is the diffraction correction for the fused silica reference echo.
- R_{w-FS} is the reflection coefficient between water and the fused silica reference sample.
- T_{ws} is the transmission coefficient between water and the sample
- k_s is the wavenumber of the sample.
- a is the transducer radius.
- ρ_w, ρ_s are the densities of the water and the sample, respectively.
- v_w, v_s are the longitudinal velocities of the water and the sample, respectively.
- α_w, α_s are the attenuation coefficients of the water and the sample, respectively.
- $C(f, x_1, y_1, z_1)$ beam focal properties.
- $P(z_1)$ corrects for time-domain window interval (equal to 1 within the interval and 0 outside of the interval).

The integral $\left[\iiint_{-\infty}^{\infty} |C(f, x_1, y_1, z_1)|^4 P(z_1) e^{-4\alpha_s z_s} dx_1 dy_1 dz_1 \right]$ is used to compensate for the transducer focusing properties.

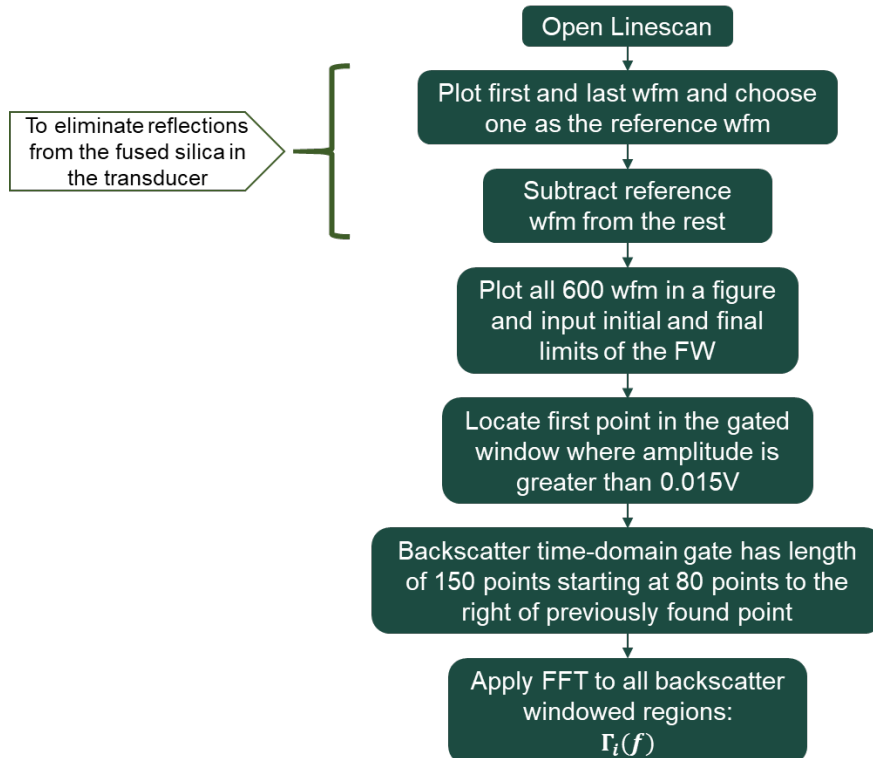


Figure A4.2. Flowchart of the processing in MATLAB to determine the backscatter noise in frequency domain per scan position.

Since all the tubes and pipe-sections have curved surfaces, a fused silica reference sample with the same dimensional characteristics must be used to obtain the final backscatter coefficient. Given that this is a comparative study between samples, that step was omitted and instead the term utilized is expressed in the next equation:

$$|\Gamma_{sample}(f)| = \sqrt{\frac{\sum_{i=1}^n |\Gamma_i(f)|^2}{n}} \dots (\text{Eq. 7})$$

Where $|\Gamma_i(f)|$ is the FFT of the windowed backscatter region in time-domain for the datapoint “*i*” of the sample and “*n*” is the number of datapoints (or scan positions) of the sample.

The rms over the frequency domain (10MHz – 40MHz) was applied to obtain a backscatter term per scan position:

$$\Gamma_{iRMS} = \sqrt{\frac{\sum_{f=10\text{MHz}}^{f=40\text{MHz}} |\Gamma_i(f)|^2}{m}} \dots (\text{Eq. 8})$$

Where “*m*” is the number of frequency discrete points from 10 to 40 MHz.

As with the attenuation coefficient processing, in this case it was also necessary to remove the blue vertical lines from the fused silica. Fig. A4.1 shows a typical backscatter experiment linescan.

The processing to determine the backscatter noise consisted in two methods: the first one to determine a backscatter RMS term in frequency domain (see Fig. A4.3), the second method to determine a backscatter coefficient as function of frequency and spatial position (see Fig. A4.4).

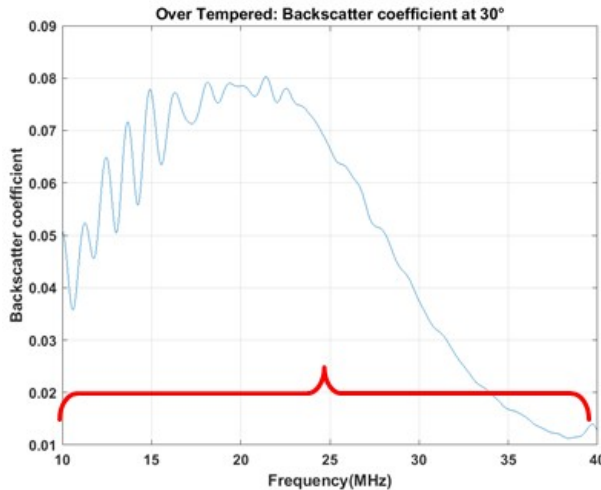


Figure A4.3. RMS in frequency domain gives a spatial backscatter term associated with each angle and each scan position.

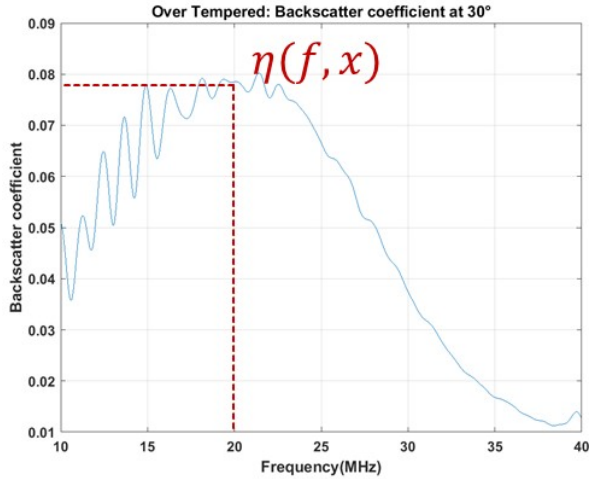
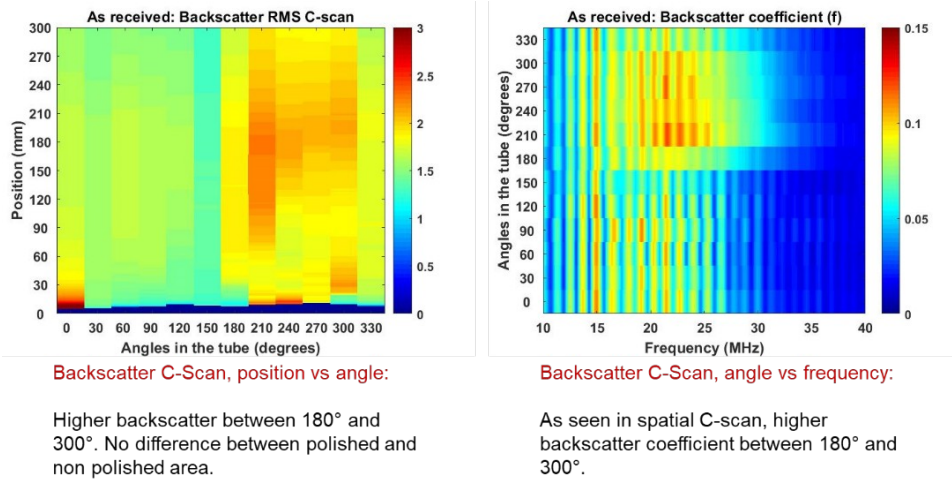
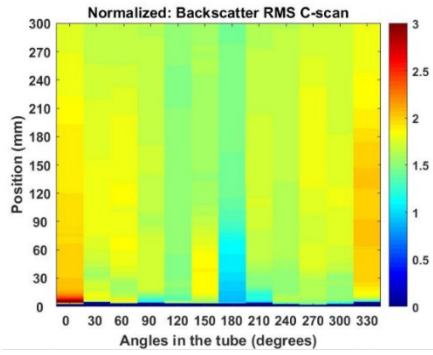


Figure A4.4. Spatial RMS along all scan points for a specific frequency, gives a backscatter coefficient as function of frequency per angle (linescan).

A4.1. BACKSCATTER NOISE RMS OF TUBE SAMPLES

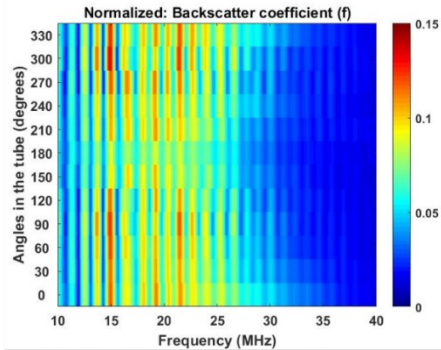
From the 7200 scan points of the tubes, backscatter rms C-scans were generated. Also, C-scans of scanned angle versus frequency is presented.





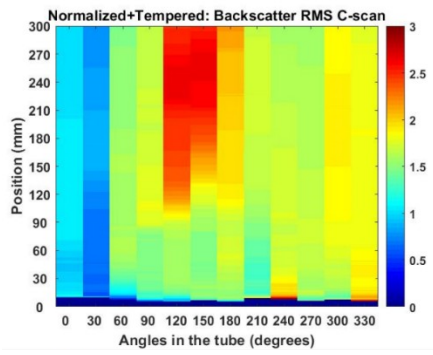
Backscatter C-Scan, position vs angle:

Between 150° and 210° there is an increase in the backscatter term after 240mm (non polished area). These values are smaller than in polished area



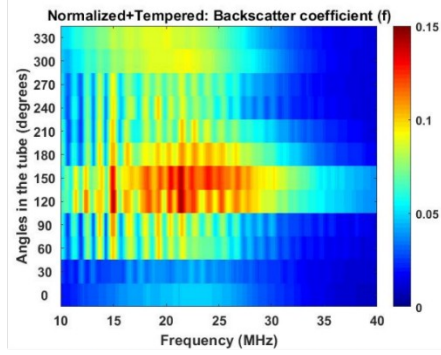
Backscatter C-Scan, angle vs frequency:

Polished area shows higher backscatter coefficient values.



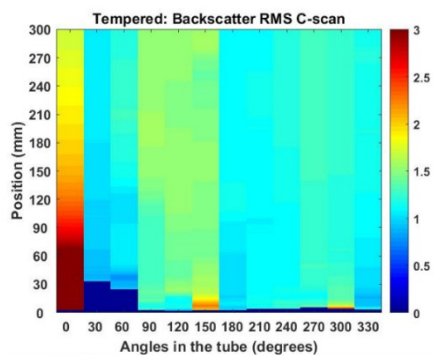
Backscatter C-Scan, position vs angle:

Higher backscatter between 120° and 180° and after 120 mm. This is not seen in the attenuation C-scan



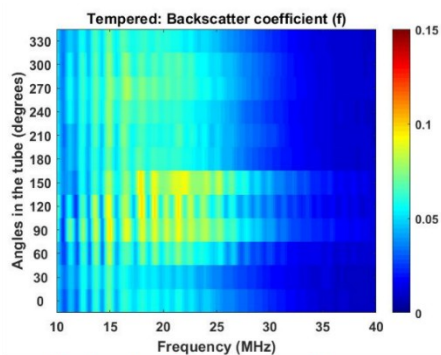
Backscatter C-Scan, angle vs frequency:

Higher backscatter between 120° and 180°.



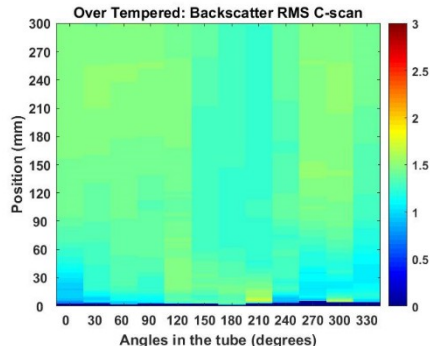
Backscatter C-Scan, position vs angle:

Higher backscatter in polished regions, between 90° and 150°. High values at 0° (to be checked).



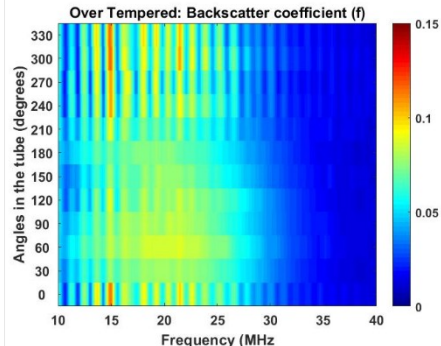
Backscatter C-Scan, angle vs frequency:

Higher attenuation in polished areas, the rest of the sample shows similar backscatter coefficients.



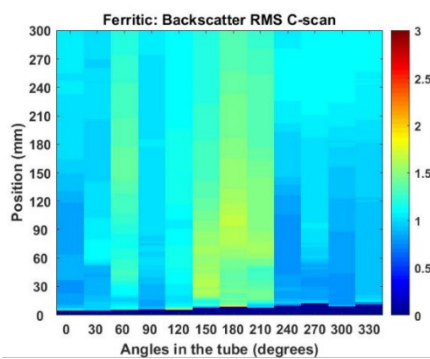
Backscatter C-Scan, position vs angle:

In general it can be seen a higher backscatter in polished areas of the sample. Small difference between polished and non polished backscatter.



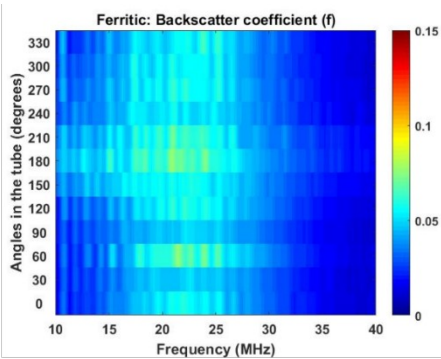
Backscatter C-Scan, angle vs frequency:

Smaller backscatter values in non polished area of the sample, between 60° and 210°.



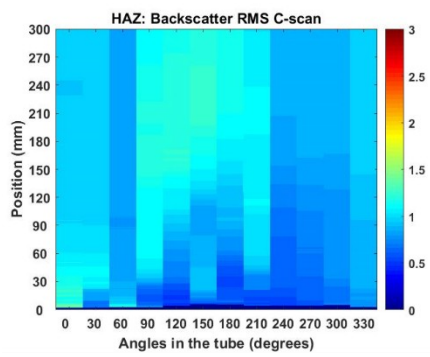
Backscatter C-Scan, position vs angle:

The higher values of backscatter are between 150° and 210°.



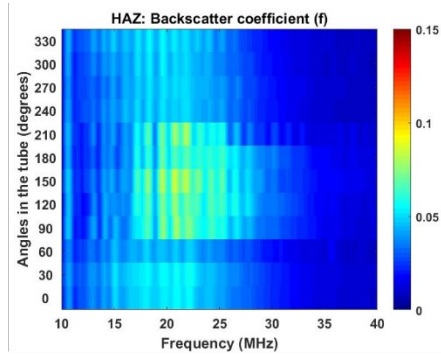
Backscatter C-Scan, angle vs frequency:

Similar as the spatial C-scan, the higher attenuation coefficient is observed between 150° and 210°.



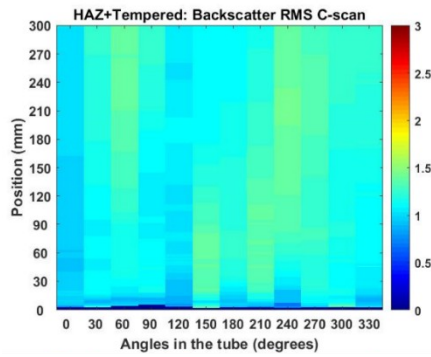
Backscatter C-Scan, position vs angle:

The polished areas show higher values of backscatter. The non polished areas show similar values.



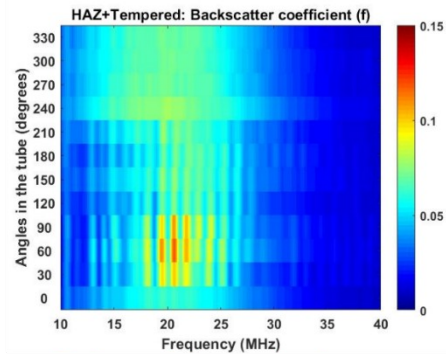
Backscatter C-Scan, angle vs frequency:

Higher backscatter coefficient in the polished areas of the sample.



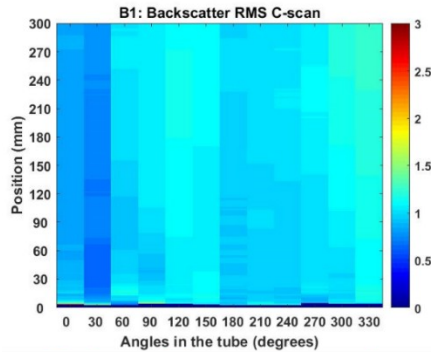
Backscatter C-Scan, position vs angle:

Small difference between polished and non polished area.



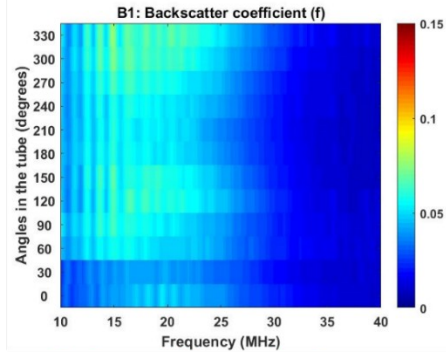
Backscatter C-Scan, angle vs frequency:

Higher attenuation between 30° and 90° .
Similar values in non polished area (after 240°).



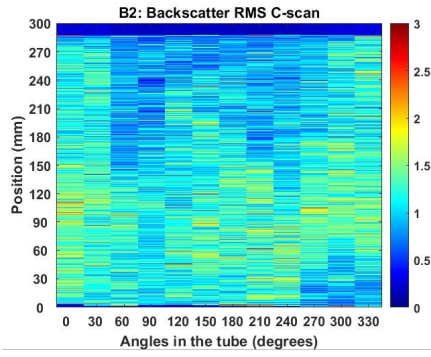
Backscatter C-Scan, position vs angle:

In general the backscatter values are similar and there is an increase after 270° .



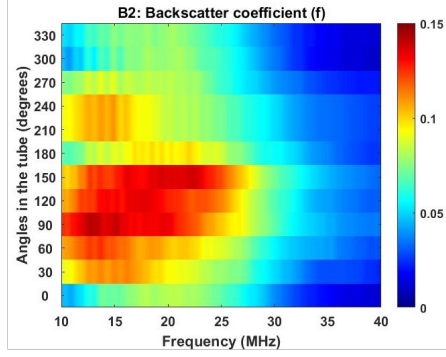
Backscatter C-Scan, angle vs frequency:

Similar values with an increase after 270° .
Low values at 0° and 30° .



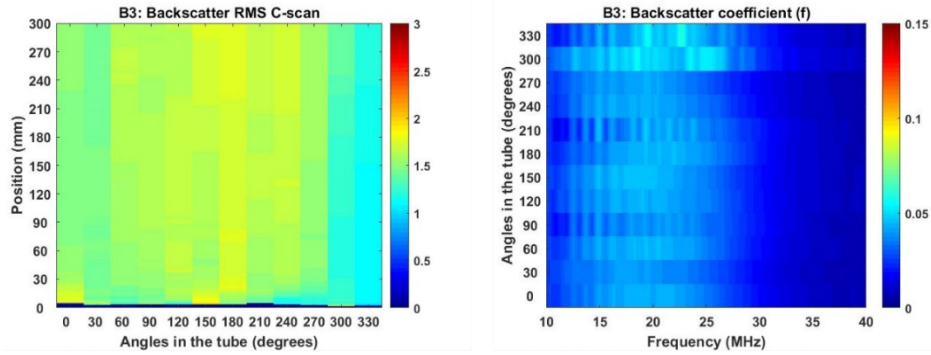
Backscatter C-Scan, position vs angle:

Similar backscatter values in all the sample with slightly higher values between 60 and 150 mm.



Backscatter C-Scan, angle vs frequency:

Higher backscatter between 60° and 150° .

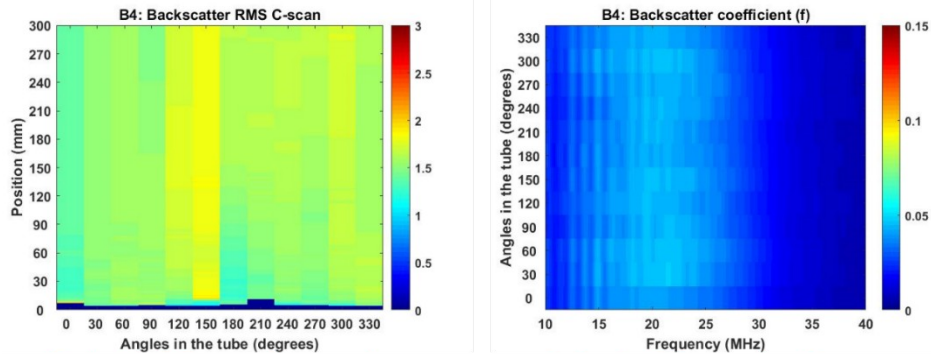


Backscatter C-Scan, position vs angle:

Similar backscatter values in all the sample.

Backscatter C-Scan, angle vs frequency:

Consistent values in all the sample with a small increase at 300° and 330°.

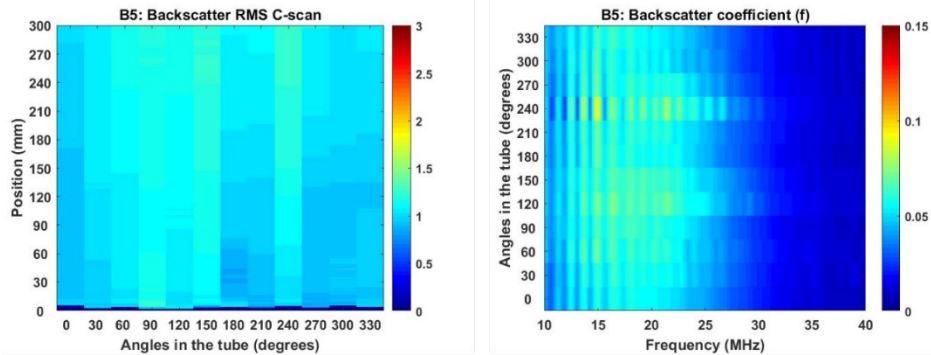


Backscatter C-Scan, position vs angle:

Similar backscatter values in all the sample.

Backscatter C-Scan, angle vs frequency:

Similar backscatter coefficient values in all the sample.

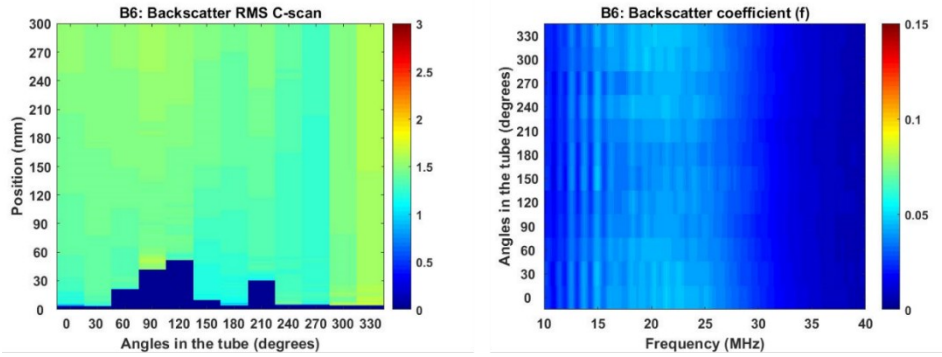


Backscatter C-Scan, position vs angle:

Similar backscatter values. The higher values are at 240° (opposite to the attenuation results).

Backscatter C-Scan, angle vs frequency:

Higher attenuation coefficient at 240°. The rest of the sample has consistent results.

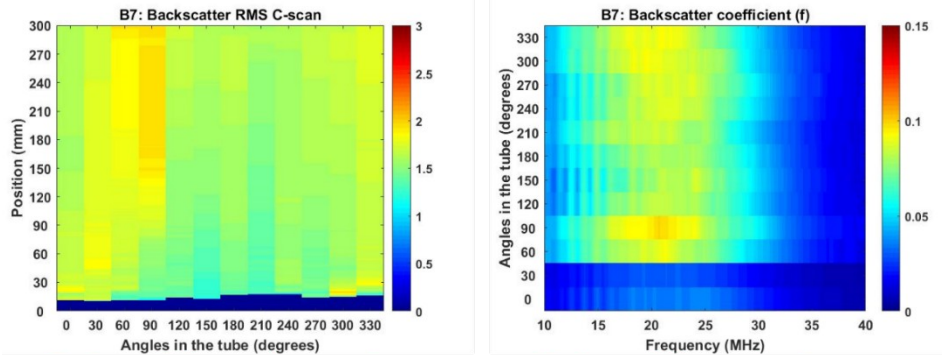


Backscatter C-Scan, position vs angle:

Almost constant value of the backscatter term along the sample. (blue areas in C-scan have zero values)

Backscatter C-Scan, angle vs frequency:

Constant backscatter coefficient in all the sample.

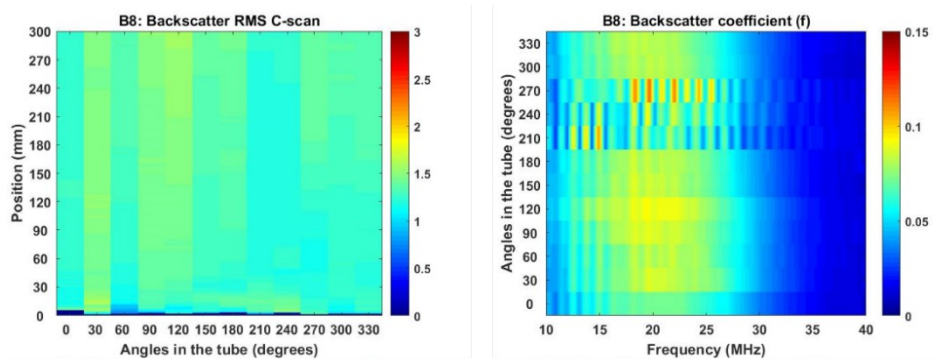


Backscatter C-Scan, position vs angle:

Almost constant backscatter values with high values between 60° and 90°.

Backscatter C-Scan, angle vs frequency:

Consistent backscatter coefficient values in all the sample except for 0° and 30°.



Backscatter C-Scan, position vs angle:

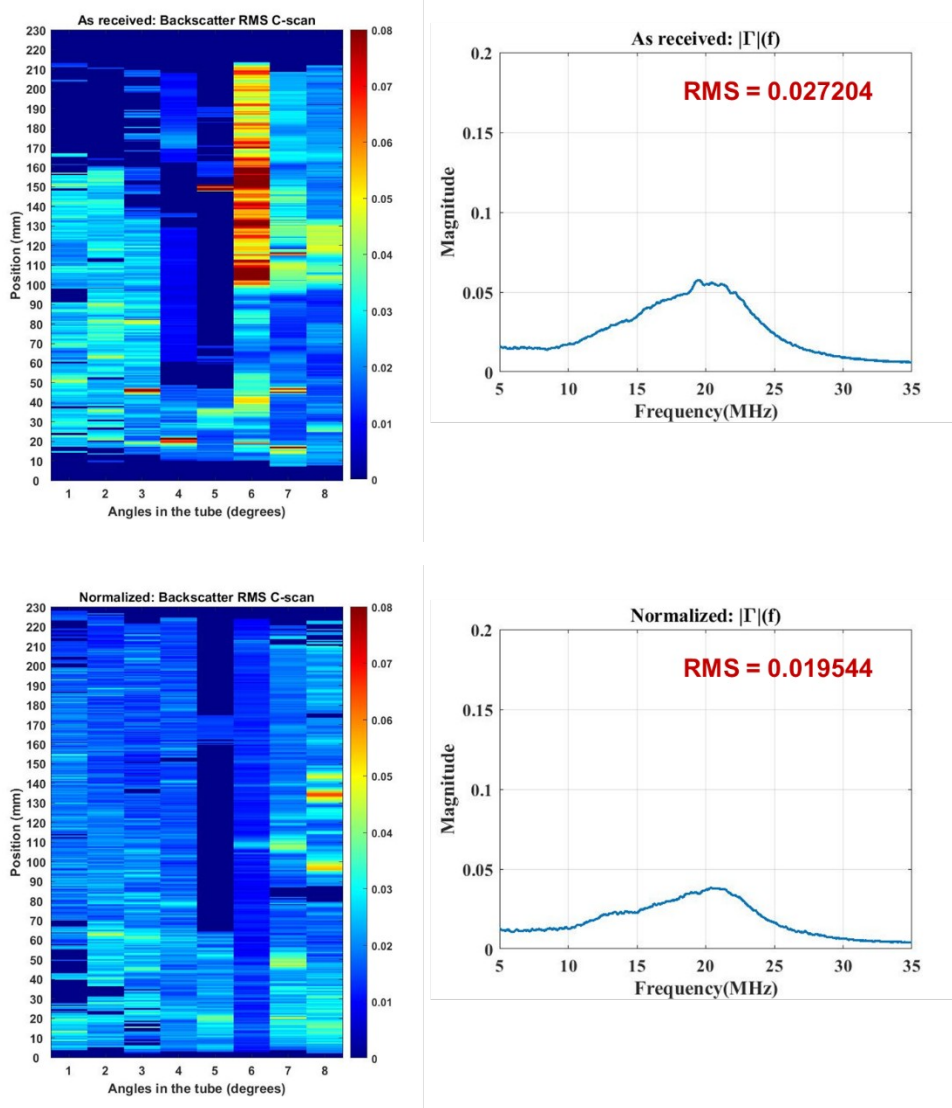
Consistent backscatter values along the sample.

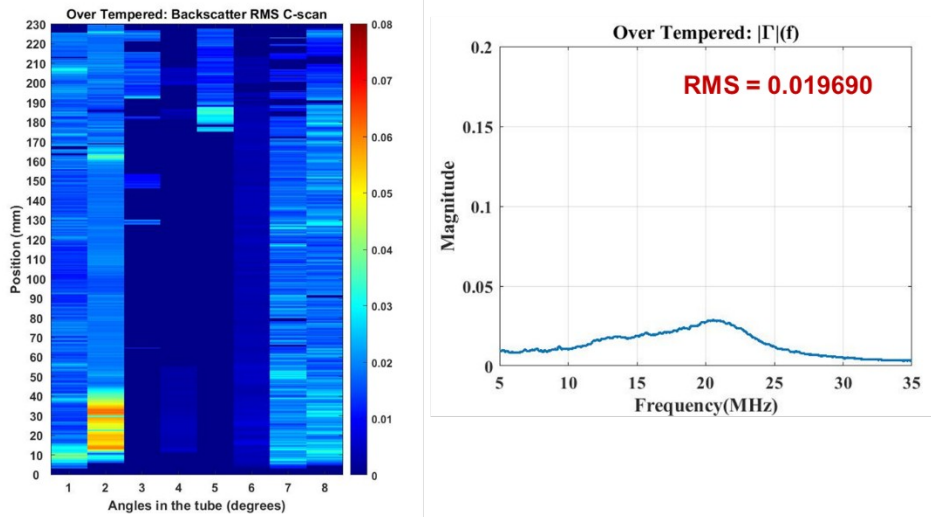
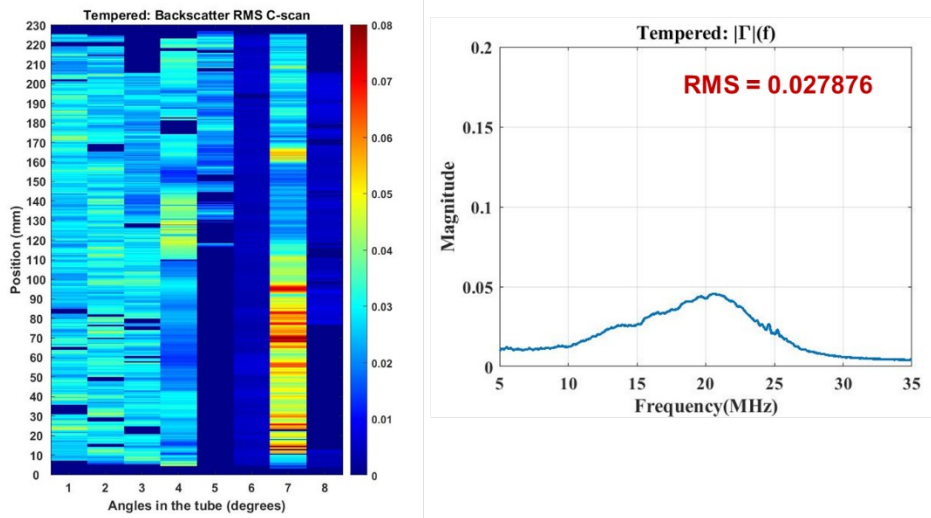
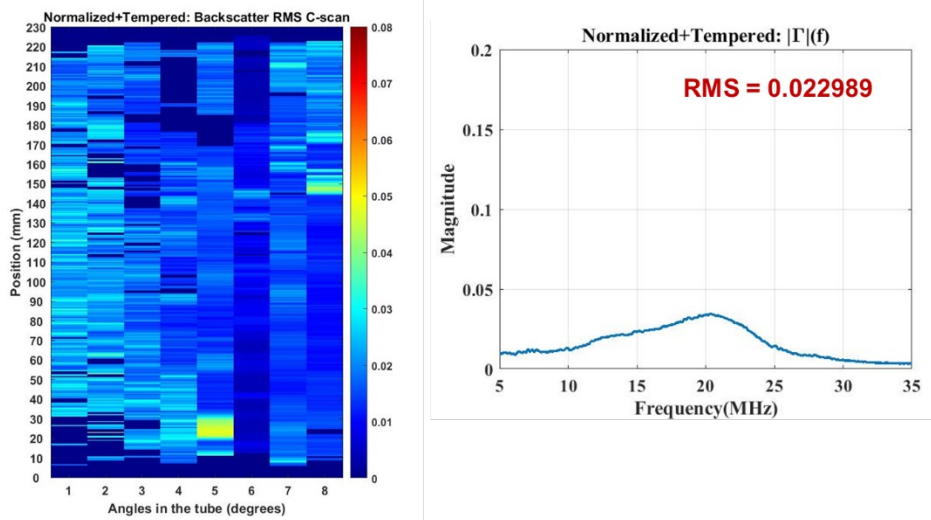
Backscatter C-Scan, angle vs frequency:

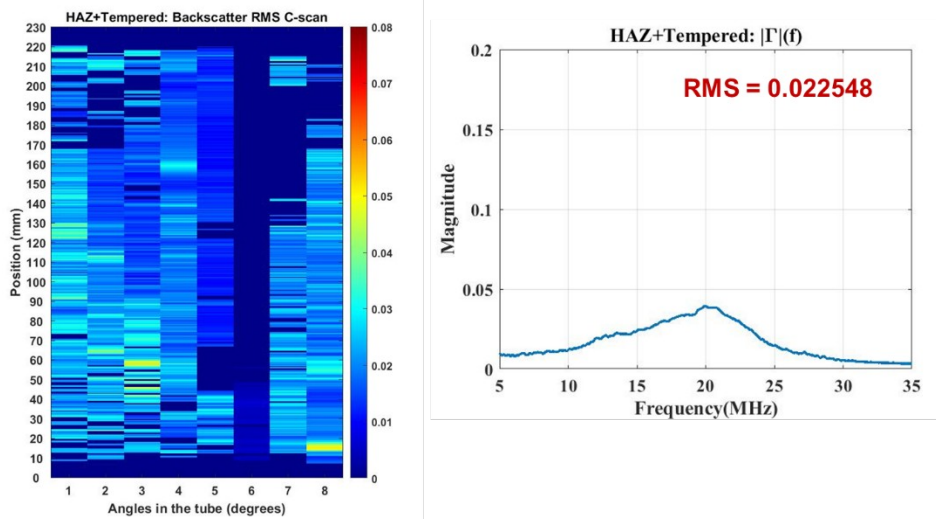
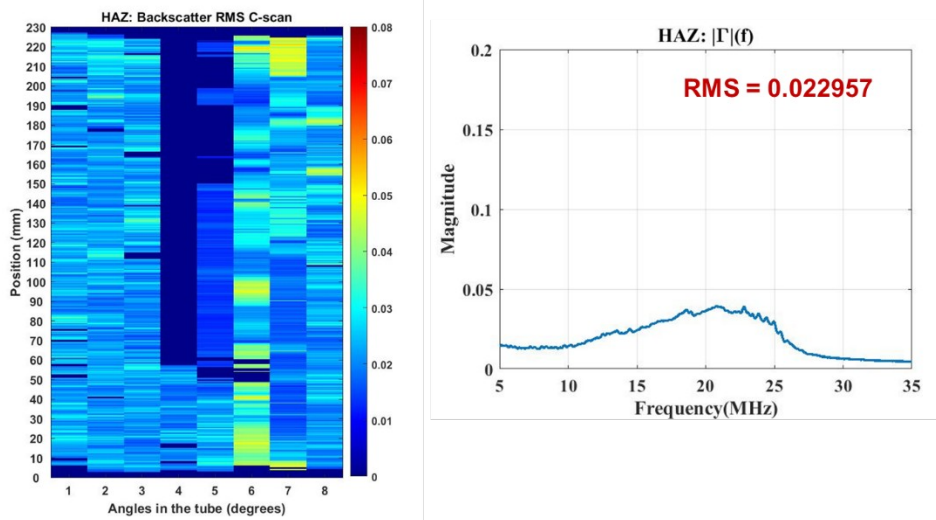
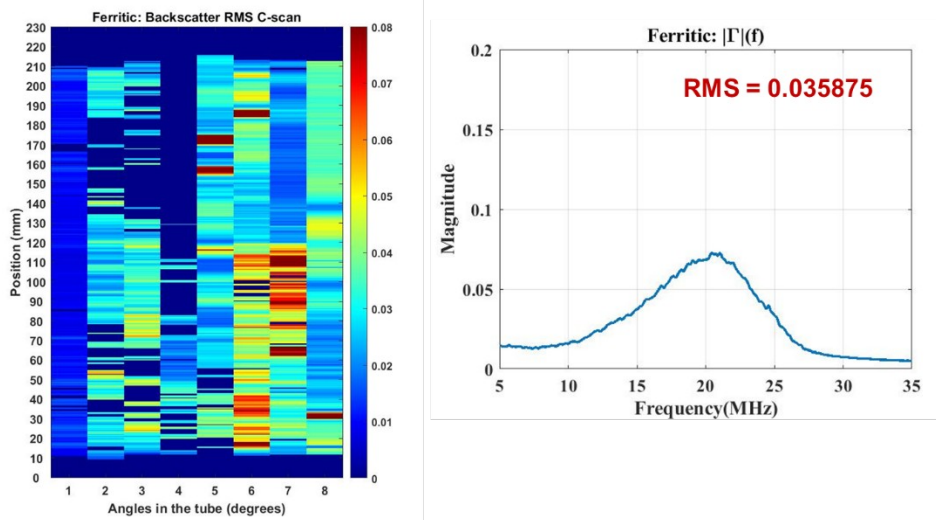
Consistent values of backscatter coefficient along the sample except in the polished area.

A4.2. BACKSCATTER NOISE RMS OF PIPE-SECTIONS

From the 3680 scan points of the pipe-sections, backscatter rms C-scans were generated. Also, the backscatter noise was averaged for each pipe-section and resulted in the backscatter noise as function of frequency. These plots are shown below:







APPENDIX 5: DETAILS OF ABSORPTION MEASUREMENT

The primary difference between the diffuse field measurement and other techniques is the *long acquisition time* in the diffuse field measurements. The current set of measurements used two 1 MHz contact transducers held a constant distance of 71 mm apart by means of a fixture, and pressed onto the surface of the tube by means of a stand. Care was taken to place the transducers in a way that the line joining the contact points was along the axis of the tube. The excitation was provided to one of the transducers by means of a square wave pulser, and the output waveform recorded at the second transducer.

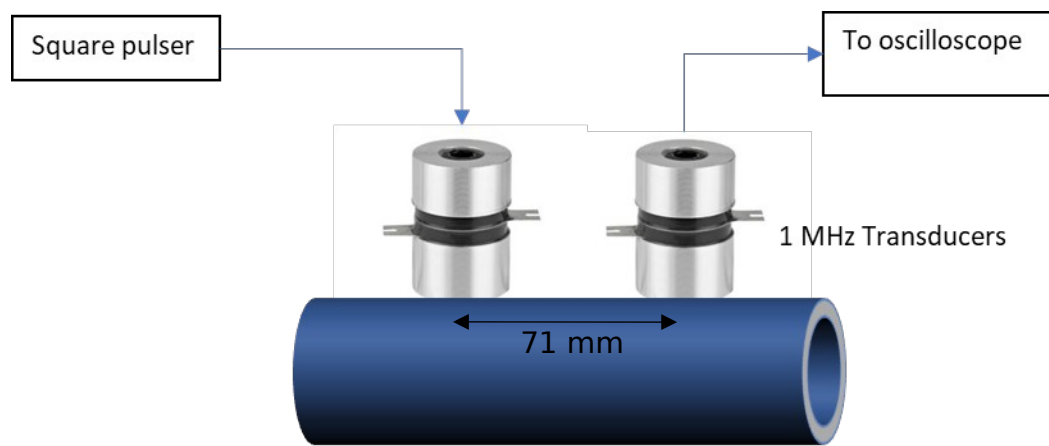


Figure A5.1: Experimental Setup for Absorption Measurement. The same setup was used for tests on the pipe sections.

The measurement was performed at 12 angular locations (30° apart) for each sample. 1 million data values were recorded for each location over a total time of 5 ms.

The same setup, described above for the tube samples, was used for the pipe cross sections and whole pipe sections. For the pipe cross sections, 3 measurements were made per sample maintaining an acquisition time of 2 ms; for the whole pipe sections, 5-9 measurements were made per sample, maintaining an acquisition time of 5 ms. A sampling rate of 1.25 GHz was maintained for these two sets of measurements. Unlike for the tubes, a constant angular increment could not be performed over the entire surface of the pipe section, and measurements were taken at locations where the transducers could be placed ensuring a relatively uniform surface pressure and contact area.

Data Processing

The data is processed using the same algorithm for the tubes, pipe cross sections, and whole pipe sections. An example of a collected output waveform is shown below.

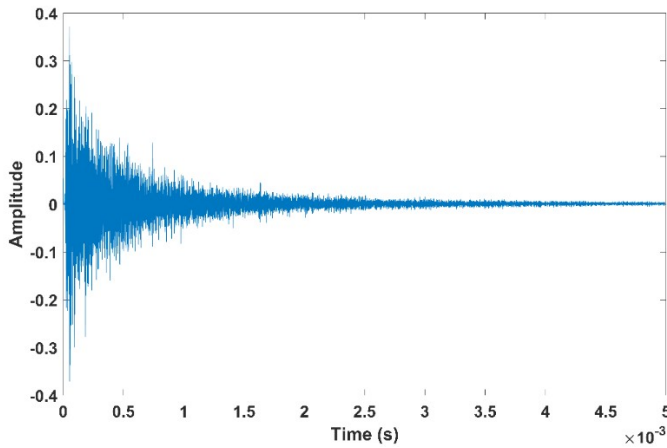


Figure A5.2: Example of output waveform (As Received sample)

It can be seen from the above figure that that the amplitude decays rapidly with time. The plots for the output waveforms for other (angular) positions on the same sample have a similar nature, and those for different samples differ in the rapidity with which the amplitude falls.

The amplitude-time output waveform is processed to finally obtain an aggregate value of the internal friction Q^{-1} for each individual sample. The steps in the data processing are detailed below.

1. For a single waveform at a chosen (angular) position, we read the amplitude-time data, and remove the initial, ‘increasing’ part of the waveform.
2. We divide the amplitude-time data into multiple segments using ‘time windows’ of user-specified length, and perform the subsequent steps for each time window, starting with the first. The chosen time windows are segmented, and we move between windows by the full length of a window.

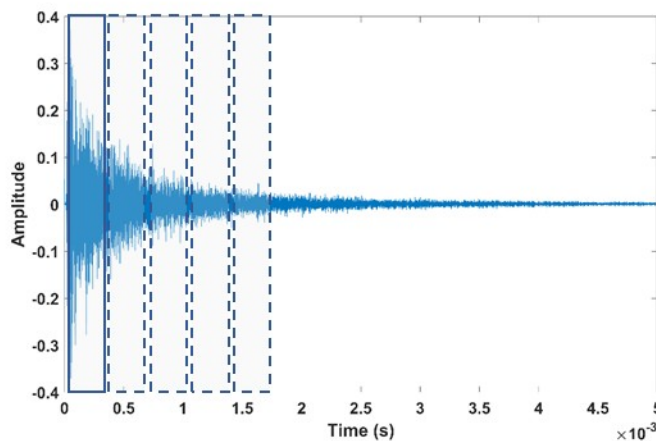


Figure A5.3: Time domain data showing the time windows

- We take the FFT of the data in the selected time window, and divide this magnitude-frequency data into multiple segments using ‘frequency windows’, again of user-specified length. We perform the subsequent steps for each frequency window, starting with the first. The chosen frequency windows are segmented, and we move between windows by the full length of a window.

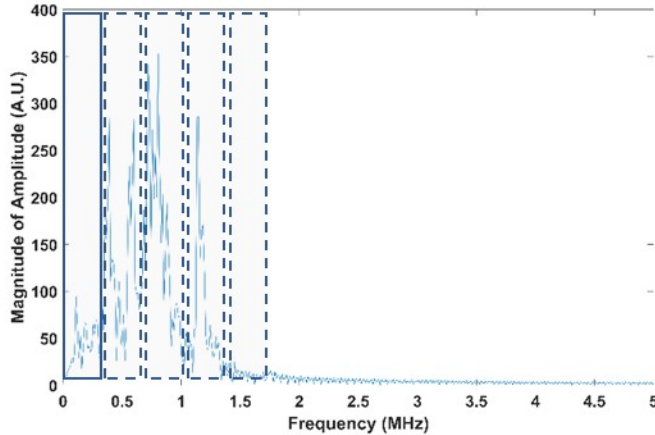


Figure A5.4: Magnitude-frequency data divided into frequency windows

- We find the ‘energy’ within a selected frequency window by calculating $E = \int |F(\omega)|^2 d\omega$
- We move on to the next frequency window and repeat step 4 for each frequency window, thereby obtaining data for the *energy at each frequency value* (chosen to be the central frequency in each window).
- We now select the next time window, and repeat steps 3 through 5 for each time window, thus obtaining the *frequency-energy data* (described in the previous step) *at each time value* (again chosen to be the central time value for each window).
- From the above-mentioned *frequency-energy data at each time value*, we now select the first frequency value.

8. We obtain the plot of *energy against time* at the chosen frequency value, and fit an exponential curve of the form $a \exp(-\sigma)$ to the energy-time plot, recording the (positive) exponential decay constant σ .

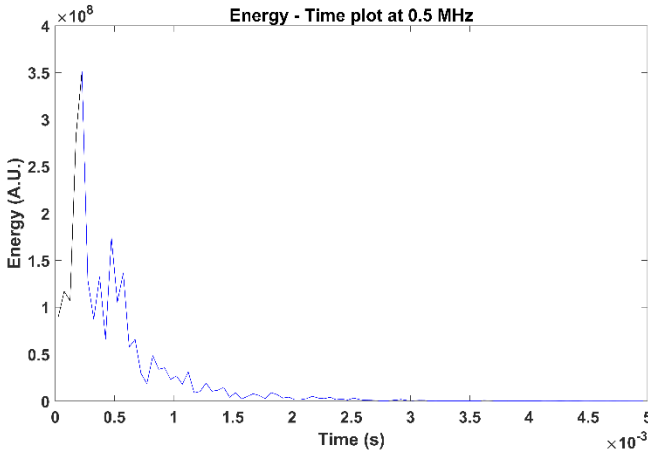


Figure A5.5: Energy-time plot

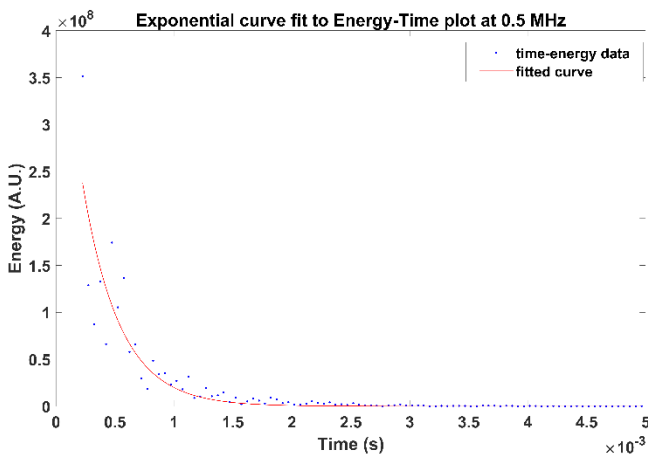


Figure A5.6: Exponential fit to energy-time plot

9. We repeat step 8 for each frequency value, recording the exponential decay constant as a function of the frequency: $\sigma(f)$. We then obtain the internal friction as a function of the frequency by

$$Q^{-1}(f) = \frac{\sigma(f)}{2\pi f}$$

10. We plot the internal friction against the frequency and identify the frequency range over which the value of Q^{-1} is roughly constant; this must roughly correspond to the bandwidth of the transducer (here, 1-3 MHz). We average the values of internal friction over the selected frequency range to obtain a measure of Q^{-1} for the chosen (angular) position.

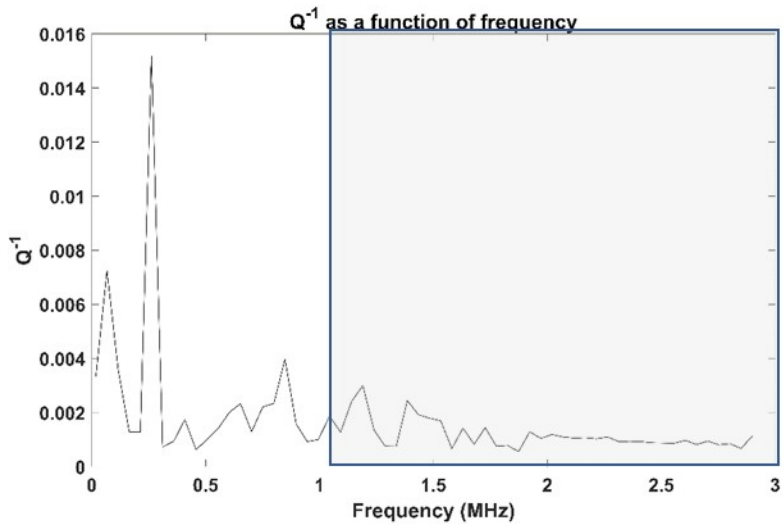


Figure A5.7: Q^{-1} -frequency plot showing the range over which Q^{-1} is roughly constant

11. We repeat steps 1 through 10 for each (angular) position on the sample to obtain Q^{-1} as a function of the (angular) position for the sample. We finally average Q^{-1} over all angles to obtain a net value of the internal friction for the sample. It is this value of the internal friction Q^{-1} that we compare across samples.

Results (Tubes)

Time window length of 50 μ s

We consider the average values of the internal friction for each sample, as shown in section 3.3.

| Sample | Value of internal friction O^{-1} | |
|-----------------------|-------------------------------------|------------------------------------|
| | Average ($\times 10^{-3}$) | Standard dev. ($\times 10^{-4}$) |
| As received | 1.257 | 2.097 |
| Fullv ferritic | 3.377 | 8.170 |
| HAZ | 1.693 | 4.597 |
| HAZ + Tempered | 1.390 | 4.182 |
| Normalized | 3.128 | 11.471 |
| Normalized + Tempered | 1.838 | 6.222 |
| Over-tempered | 1.526 | 4.334 |
| Tempered | 1.611 | 8.729 |

| Sample | Value of internal friction O^{-1} | |
|--------|-------------------------------------|------------------------------------|
| | Average ($\times 10^{-3}$) | Standard dev. ($\times 10^{-4}$) |
| | | |

| | | |
|----|-------|-------|
| B1 | 1.264 | 5.194 |
| B2 | 2.486 | 8.156 |
| B3 | 1.168 | 5.554 |
| B4 | 2.084 | 6.480 |
| B5 | 1.141 | 4.475 |
| B6 | 1.323 | 5.744 |
| B7 | 1.908 | 9.261 |
| B8 | 0.933 | 3.036 |

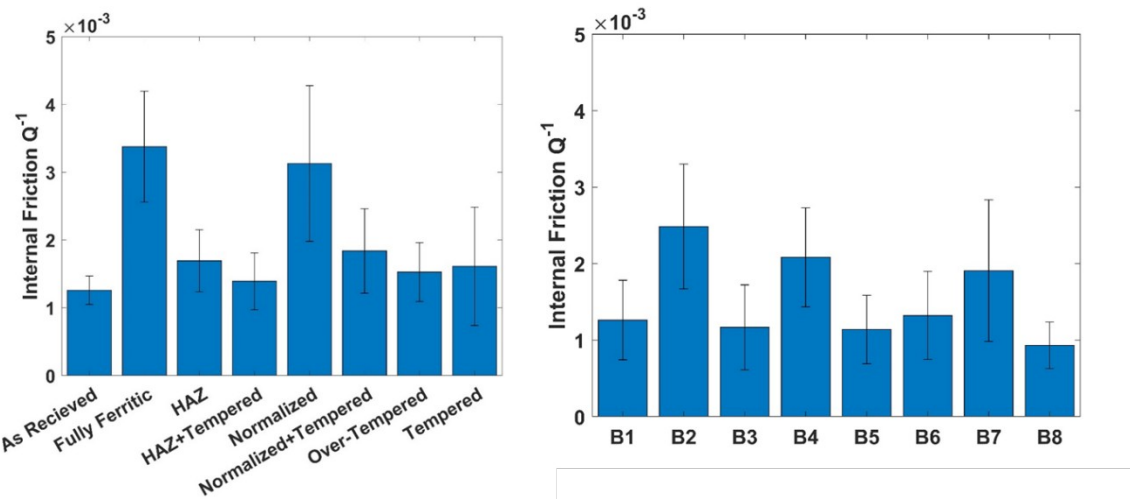


Figure A5.8: Aggregated values of Q^{-1} for the tube samples considering a time window length of 50 μs
Time window length of 100 μs

We consider the average values of the internal friction for each sample, shown in tabular and chart format for this and all subsequent cases.

| Sample | Value of internal friction O^{-1} | |
|-----------------------|--|------------------------------------|
| | Average ($\times 10^{-4}$) | Standard dev. ($\times 10^{-4}$) |
| As received | 9.824 | 3.254 |
| Fully ferritic | 8.660 | 2.764 |
| HAZ | 10.512 | 4.370 |
| HAZ + Tempered | 7.883 | 3.172 |
| Normalized | 9.585 | 1.753 |
| Normalized + Tempered | 12.873 | 3.296 |
| Over-tempered | 7.800 | 2.345 |
| Tempered | 7.416 | 2.868 |

| Sample | Value of internal friction O^{-1} |
|--------|--|
| | |

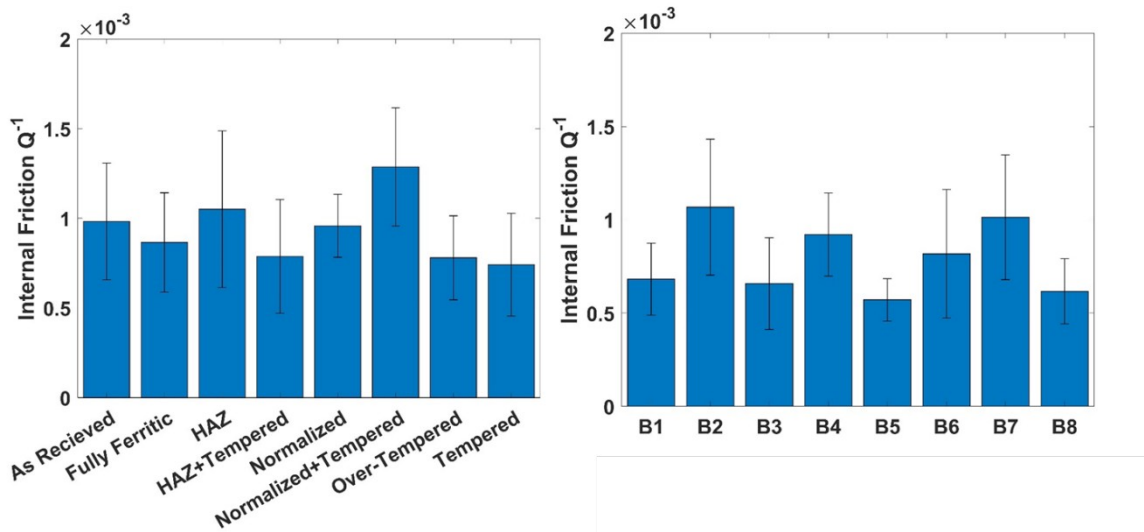


Figure A5.9: Aggregated values of Q^{-1} for the tube samples considering a time window length of 100 μs

Time window length of 200 μs

We consider the average values of the internal friction for each sample, as previously.

| Sample | Value of internal friction O^{-1} | |
|-----------------------|--|------------------------------------|
| | Average ($\times 10^{-4}$) | Standard dev. ($\times 10^{-5}$) |
| As received | 4.882 | 8.135 |
| Fully ferritic | 6.568 | 8.823 |
| HAZ | 4.252 | 6.627 |
| HAZ + Tempered | 4.936 | 17.576 |
| Normalized | 6.567 | 6.239 |
| Normalized + Tempered | 8.345 | 16.489 |
| Over-tempered | 4.764 | 11.409 |
| Tempered | 3.838 | 4.129 |

| Sample | Value of internal friction O^{-1} | |
|--------|--|------------------------------------|
| | Average ($\times 10^{-4}$) | Standard dev. ($\times 10^{-5}$) |
| B1 | 3.725 | 9.437 |
| B2 | 8.744 | 23.438 |
| B3 | 3.494 | 7.753 |
| B4 | 7.006 | 13.570 |
| B5 | 3.974 | 8.808 |

| | | |
|----|-------|--------|
| B6 | 4.008 | 10.974 |
| B7 | 5.251 | 7.959 |
| B8 | 4.160 | 9.148 |

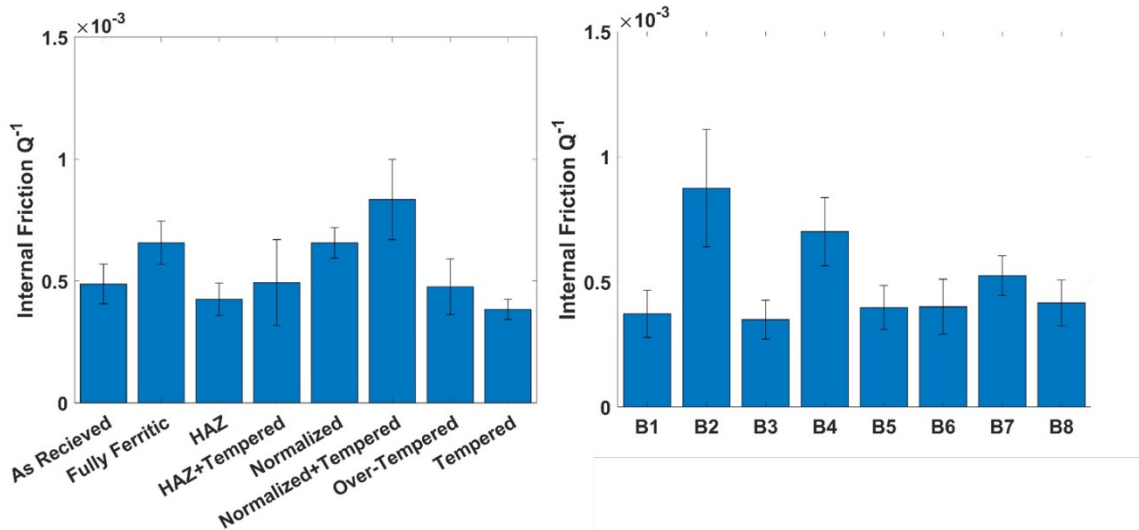


Figure A5.10: Aggregated values of Q^{-1} for the tube samples considering a time window length of 200 μs

Time window length of 500 μs

We consider the average values of the internal friction for each sample, as previously.

| Sample | Value of internal friction O^{-1} | |
|-----------------------|-------------------------------------|------------------------------------|
| | Average ($\times 10^{-4}$) | Standard dev. ($\times 10^{-5}$) |
| As received | 2.833 | 2.266 |
| Fully ferritic | 4.931 | 6.446 |
| HAZ | 3.486 | 2.748 |
| HAZ + Tempered | 3.551 | 11.130 |
| Normalized | 4.431 | 7.462 |
| Normalized + Tempered | 5.302 | 6.570 |
| Over-tempered | 3.320 | 3.053 |
| Tempered | 2.831 | 2.818 |

| Sample | Value of internal friction O^{-1} | |
|--------|-------------------------------------|-----------------------|
| | Average ($\times 10^{-4}$) | Standard dev (x10^-5) |
| B1 | 2.335 | 1.804 |

| | | |
|----|-------|--------|
| B2 | 5.706 | 13.852 |
| B3 | 2.435 | 2.995 |
| B4 | 3.787 | 9.973 |
| B5 | 2.299 | 3.349 |
| B6 | 2.400 | 2.590 |
| B7 | 4.056 | 8.393 |
| B8 | 3.193 | 7.637 |

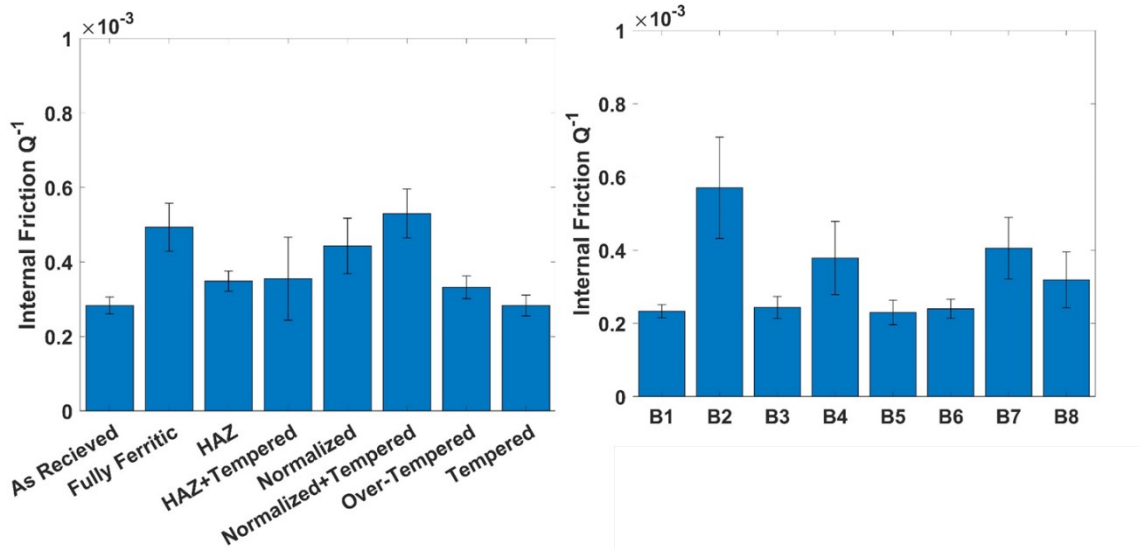


Figure A5.11: Aggregated values of Q^{-1} for the tube samples considering a time window length of 500 μs

Results (Pipe Cross-sections)

We consider the average values of internal friction for each pipe cross-section sample. The results are presented for time window lengths of 50 μs and 100 μs , with a constant frequency window length of 50 kHz.

Time window length of 50 μs

| Sample | Value of internal friction O^{-1} | |
|----------------|--|------------------------------------|
| | Average ($\times 10^{-3}$) | Standard dev. ($\times 10^{-4}$) |
| As received | 1.802 | 3.590 |
| Ferritic | 2.074 | 3.322 |
| HAZ | 2.127 | 1.826 |
| HAZ + Tempered | 2.830 | 2.549 |
| Normalized | 2.581 | 1.979 |

| | | |
|-----------------------|-------|-------|
| Normalized + Tempered | 2.228 | 3.194 |
| Over-tempered | 2.388 | 1.537 |
| Tempered | 2.278 | 7.388 |

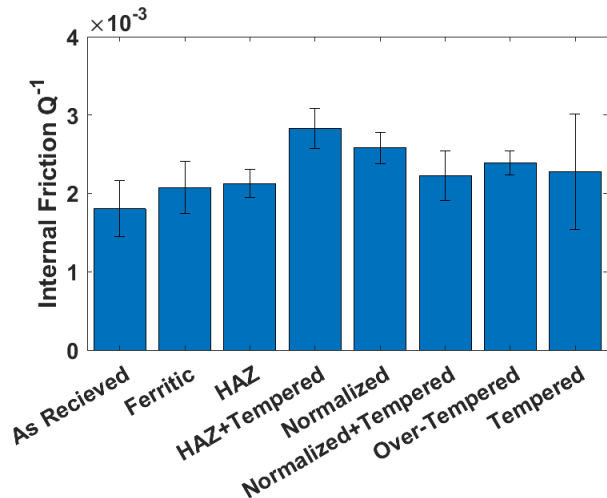


Figure A5.12: Aggregated values of Q^{-1} for the pipe cross sections considering a time window length of 50 μs

Time window length of 100 μs

| Sample | Value of internal friction Q^{-1} | |
|-----------------------|-------------------------------------|------------------------------------|
| | Average ($\times 10^{-3}$) | Standard dev. ($\times 10^{-4}$) |
| As received | 0.929 | 0.669 |
| Ferritic | 1.168 | 1.108 |
| HAZ | 1.124 | 0.713 |
| HAZ + Tempered | 1.001 | 1.409 |
| Normalized | 1.440 | 2.013 |
| Normalized + Tempered | 1.043 | 3.667 |
| Over-tempered | 1.261 | 2.746 |
| Tempered | 1.644 | 6.066 |

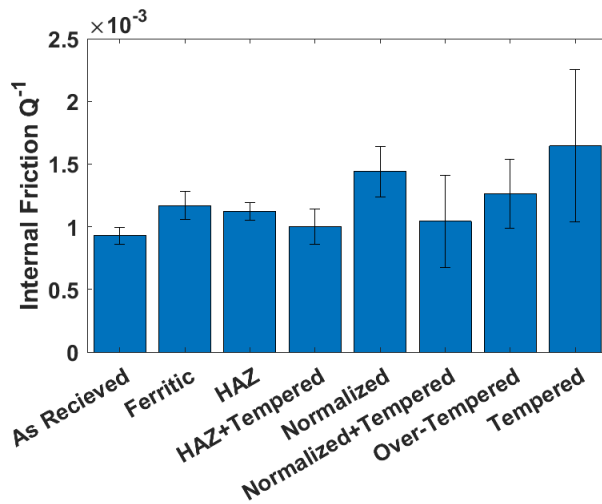


Figure A5.13: Aggregated values of Q^{-1} for the pipe cross sections considering a time window length of 100 μs

Results (Whole Pipe Sections)

We consider the average values of internal friction for each pipe section sample. The results are presented for time window lengths of 50 μs and 100 μs , with a constant frequency window length of 50 kHz.

Time window length of 50 μs

| Sample | Value of internal friction O^{-1} | |
|-----------------------|--|------------------------------------|
| | Average ($\times 10^{-3}$) | Standard dev. ($\times 10^{-4}$) |
| As received | 2.499 | 6.450 |
| Ferritic | 1.802 | 7.865 |
| HAZ | 1.627 | 4.374 |
| HAZ + Tempered | 1.935 | 3.591 |
| Normalized | 2.016 | 6.738 |
| Normalized + Tempered | 2.380 | 7.942 |
| Over-tempered | 1.690 | 7.020 |
| Tempered | 2.338 | 4.970 |

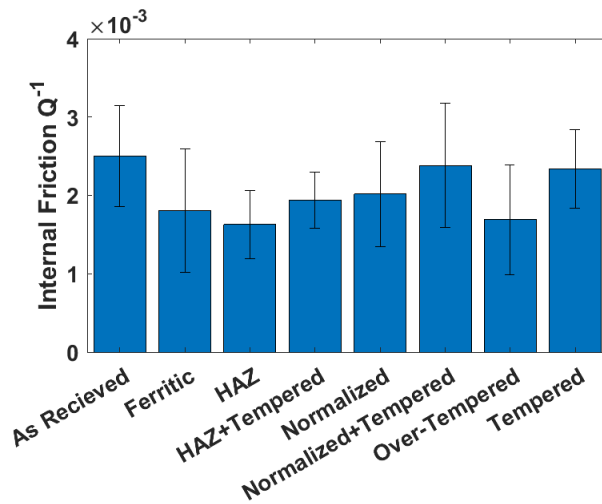


Figure A5.14: Aggregated values of Q^{-1} for the pipe sections considering a time window length of 50 μs

Time window length of 100 μs

| Sample | Value of internal friction O^{-1} | |
|-----------------------|-------------------------------------|------------------------------------|
| | Average ($\times 10^{-4}$) | Standard dev. ($\times 10^{-4}$) |
| As received | 9.161 | 2.890 |
| Ferritic | 7.184 | 1.779 |
| HAZ | 6.181 | 0.702 |
| HAZ + Tempered | 8.020 | 2.274 |
| Normalized | 7.228 | 2.129 |
| Normalized + Tempered | 9.835 | 4.739 |
| Over-tempered | 6.765 | 1.968 |
| Tempered | 10.943 | 2.541 |

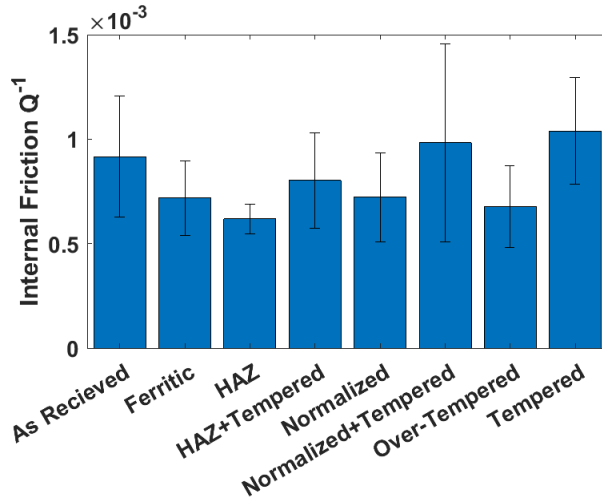
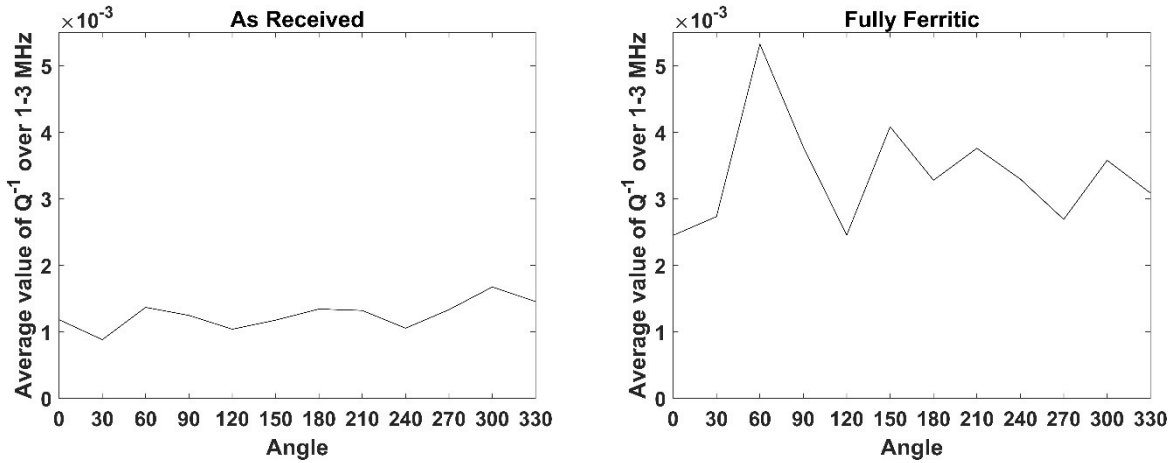
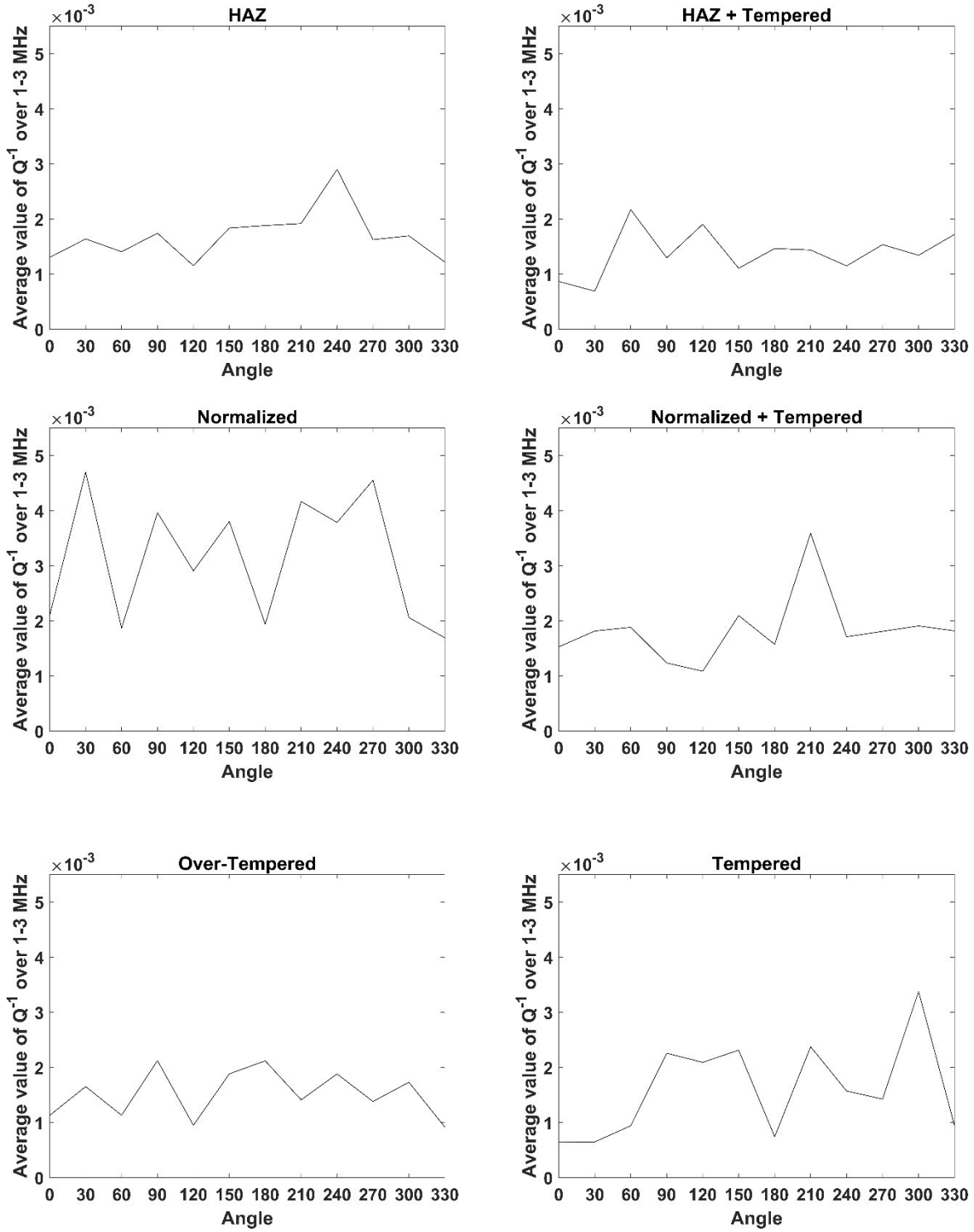


Figure A5.15: Aggregated values of Q^{-1} for the pipe sections considering a time window length of 100 μ s

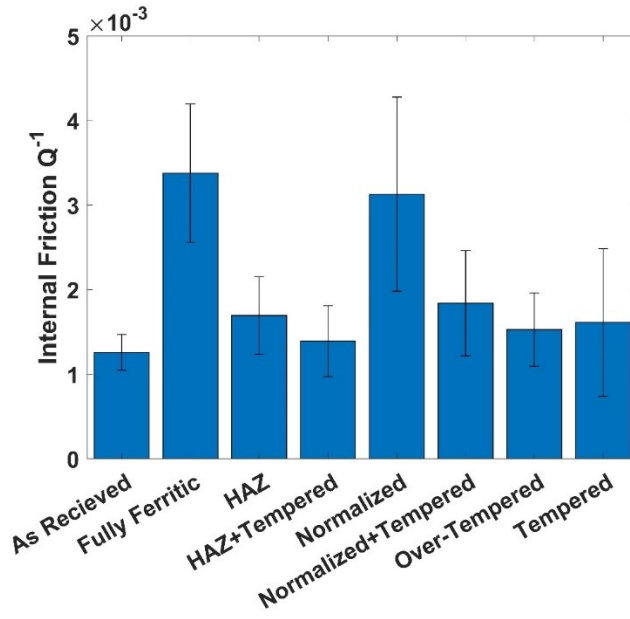
Discussion

We consider the causes of the error in the value of the internal friction Q^{-1} . We first look at plots of Q^{-1} (calculated in the bandwidth 1-3 MHz) versus the angular position in the known tube samples. These plots have been obtained at a time window length of 50 μ s, and a frequency window length of 50 kHz. Similar plots can be obtained for other choices of the window lengths, and for the other classes of the samples.



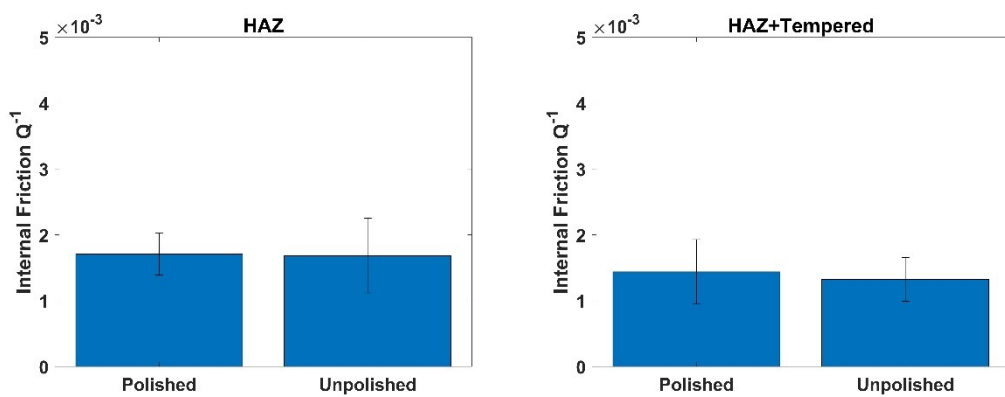


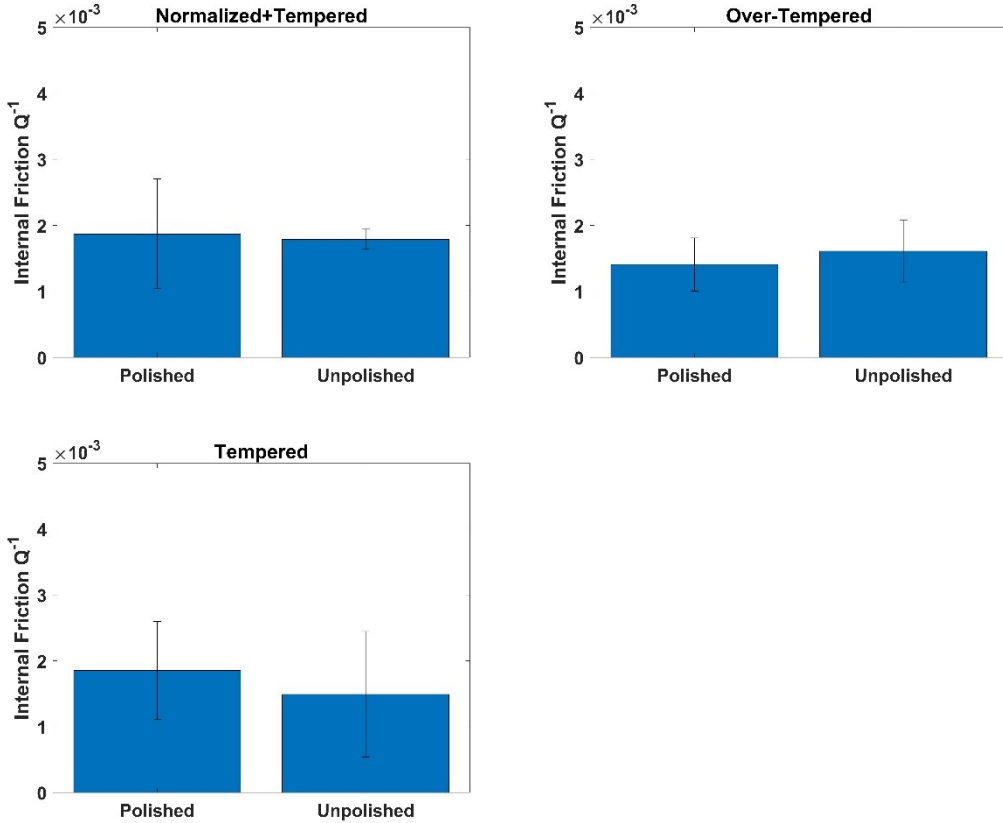
The averaged values of Q^{-1} over all angles for this case, along with error bars indicating their (standard deviation spread) is shown once again.



The spread in the values of Q^{-1} with the angle could be due to:

- Variation in the nature of the contact between the transducers and the tube surface or pipe section surface. There is an improper contact due to the flat surface of the transducers mating, through a layer of couplant, with the curved surface of the tubes and pipe sections. It is very likely that there were variations in the locations of the transducers and in the pressure with which they were held to the surface. Further, the surface of the pipe sections was not of uniform curvature; there were flat spots at various locations of the sample/
- Variations in the *surface conditions* at different angular locations on the same tube or pipe section. It may be expected that the measurements taken at polished regions of the sample will differ from those taken at the unpolished regions. This, however, was found not to be true by considering the average values of Q^{-1} across polished and unpolished regions of samples (where they arose) separately, and comparing them. The results shown below for the known tubes, but hold for the other samples as well.





It can be seen that there is no observable difference between the values of Q^{-1} as recorded at the polished and the unpolished regions once the deviations in the values are taken into account.

- Difference in the material property itself at different angular positions on the same tube. Any such differences are expected to be marginal.

It can be concluded that the errors in the values of Q^{-1} must be chiefly due to the variations in the experimental conditions (points of contact, pressure applied on the transducers, thickness and uniformity of the couplant layer, etc.).

We also note that variations in the selected time window length lead to different final values of the internal friction Q^{-1} being calculated for each sample. Judicious choice of the time window length is essential to obtain reasonable results.